

MARTIN MARIETTA ENERGY SYSTEMS LIBRARIES
3 4456 0134149 6

CENTRAL RESEARCH LIBRARY
DOCUMENT COLLECTION

113110 ✓

ORNL-3506
UC-34 - Physics
TID-4500 (37th ed.)

SPECTRA OF GAMMA RAYS PRODUCED BY THE
INTERACTION OF ~160-MeV PROTONS WITH
Be, C, O, Al, Co, AND Bi

W. Zobel
F. C. Maienschein
R. J. Scroggs



OAK RIDGE NATIONAL LABORATORY
operated by
UNION CARBIDE CORPORATION
for the
U.S. ATOMIC ENERGY COMMISSION

**CENTRAL RESEARCH LIBRARY
DOCUMENT COLLECTION
LIBRARY LOAN COPY**
DO NOT TRANSFER TO ANOTHER PERSON
If you wish someone else to see this
document, send in name with document
and the library will arrange a loan.

Printed in USA. Price \$3.00. Available from the Clearinghouse for Federal
Scientific and Technical Information, National Bureau of Standards,
U.S. Department of Commerce, Springfield, Virginia

— LEGAL NOTICE —

This report was prepared as an account of Government sponsored work. Neither the United States, nor the Commission, nor any person acting on behalf of the Commission:

- A. Makes any warranty or representation, expressed or implied, with respect to the accuracy, completeness, or usefulness of the information contained in this report, or that the use of any information, apparatus, method, or process disclosed in this report may not infringe privately owned rights; or
- B. Assumes any liabilities with respect to the use of, or for damages resulting from the use of any information, apparatus, method, or process disclosed in this report.

As used in the above, "person acting on behalf of the Commission" includes any employee or contractor of the Commission, or employee of such contractor, to the extent that such employee or contractor of the Commission, or employee of such contractor prepares, disseminates, or provides access to, any information pursuant to his employment or contract with the Commission, or his employment with such contractor.

ORNL-3506

Contract No. W-7405-eng-26

Neutron Physics Division

SPECTRA OF GAMMA RAYS PRODUCED BY THE INTERACTION OF
~ 160-MeV PROTONS WITH Be, C, O, Al, Co, AND Bi

W. Zobel, F. C. Maienschein, and R. J. Scroggs*

Note:

This Work Supported by
NATIONAL AERONAUTICS AND SPACE ADMINISTRATION
Under Order R-104

APRIL 1965

OAK RIDGE NATIONAL LABORATORY
Oak Ridge, Tennessee
operated by
UNION CARBIDE CORPORATION
for the
U.S. ATOMIC ENERGY COMMISSION



3 4456 0134149 6

*Instrumentation and Controls Division; now at Oak Ridge Technical
Enterprises Corp., Oak Ridge, Tennessee.



Table of Contents

	<u>Page No.</u>
Abstract -----	1
I. Introduction -----	1
II. Apparatus -----	4
A. Gamma-Ray Spectrometer -----	4
B. Neutron Rejection by Time of Flight -----	10
C. Discussion of Electronics Block Diagram -----	15
D. Beam Monitor and Control Circuit -----	27
E. Target Description -----	29
F. Disposition at Synchrocyclotron -----	30
III. Calibrations -----	32
A. Gain and Gain Shift with Count Rate -----	32
B. Coincidence Circuit Time Resolution and Counting Efficiency -----	35
C. Chance Coincidence Backgrounds -----	37
D. Count Losses -----	38
E. Spectrometer Efficiency -----	41
F. Neutron Rejection Efficiency -----	45
IV. Results and Discussion -----	53
A. Data Analysis -----	53
B. Spectra and Cross Sections at 136° -----	55
C. Spectra at Other Angles -----	68
D. Further Studies -----	69
V. Acknowledgments -----	72

SPECTRA OF GAMMA RAYS PRODUCED BY THE INTERACTION OF
~ 160-MeV PROTONS WITH Be, C, O, Al, Co, AND Bi

W. Zobel, F. C. Maienschein, and R. J. Scroggs*

Abstract

A measurement of the gamma rays in the energy range from 0.6 MeV to 11 MeV resulting from bombardment of Be, C, H₂O, Al, Co, and Bi targets with ~ 160-MeV protons has been completed. A three-crystal scintillation spectrometer was used as a pair spectrometer for photons having energies above 2 MeV and as a total-absorption, anticoincidence spectrometer for photons having energies below 2.5 MeV. A time-of-flight method was used to reject counts due to neutrons, with an average rejection efficiency of 0.70 ± 0.01 . Data were obtained in the form of pulse-height spectra which were converted to photon spectra by a computer-programmed "unscrambling" technique resulting in the assignment of upper and lower spectral bounds representing a 68% confidence interval. The bulk of the data was obtained at 136° from the direction of the proton beam; other data obtained with aluminum targets at 44° and 20.5° give no evidence of anisotropy.

Discrete gamma rays were found for all materials except bismuth. Cross sections for the production of these gamma rays were computed and plausible assignments were made for the transitions giving rise to these lines. In the case of Al, Co, and Bi a continuum was observed, underlying the discrete spectrum for the aluminum and cobalt targets.

The total gamma-ray production cross sections for photons in the energy range from 0.6 MeV to 11 MeV were calculated to be: Be, (6.8 ± 1.3) mb; C, (41.4 ± 6.3) mb; O, (115 ± 22) mb; Al, (434 ± 97) mb; and Co, (1050 ± 220) mb. Where comparisons with the work of other investigators are available, the present cross-section results appear to be, in general, somewhat larger.

I. Introduction

The nuclear secondaries produced by the interaction of high-energy protons with nuclei are of interest since protons are the most abundant of the charged particles in space which present a hazard for manned space travel. Spacecraft shields, which are presently envisaged as necessary for protection on interplanetary flights or for high-altitude orbiting

*Oak Ridge Technical Enterprises Corp., Oak Ridge, Tennessee.

stations, are of such thickness that the biological damage produced by secondaries from nuclear interactions in the shield becomes important compared with that produced by ionization by the primary protons. The secondaries may be uncharged, and thus more penetrating than the primaries, and they may produce greater biological damage. Thus their production and transport in the spacecraft shield or structure must be carefully assessed.

The application of a simple nuclear model, which assumes interaction of the incoming proton with a single nucleon, appears to give predictions of secondary nucleon spectra which are in reasonable agreement with experiments for $Z > 12$ and proton energies from 50 MeV to 2 BeV.¹ The energy distributions of the residual nuclei are available from this calculation and from the complementary evaporation calculation which is used to treat nucleons below 50 MeV. However, these data have not yet been used to predict the gamma-ray spectra from proton bombardment. Hill and Simpson² have used a statistical estimate of the population densities of the energy levels of the residual nuclei in an attempt to predict such spectra, but results are not yet available for detailed comparison. Thus, in order to calculate the effect of secondary gamma-ray emission, measurements of cross sections for the production of gamma-ray transitions of specified energy are needed.

As part of a larger effort to study secondaries,³ measurements were made of the gamma rays produced by 160-MeV protons from the Harvard University synchrocyclotron in targets of Be, C, H₂O, Al, Co, and Bi. In addition, measurements were made with an aluminum target thick compared to the range of the protons. These latter data were obtained to test the calculation by Monte Carlo techniques of the transport of the gamma rays through a "thick" target.

-
1. H. W. Bertini, Phys. Rev. 131, 1801 (1963).
 2. C. W. Hill and K. M. Simpson, Jr., Calculation of Proton-Induced Gamma-Ray Spectrum and Comparison with Experiment, Second Symposium on Protection Against Radiation Hazards in Space, Gatlinburg, Tenn., Oct. 12-14, 1964.
 3. Neutron Phys. Div. Ann. Progr. Rept. Aug. 31, 1962, Vol. II, ORNL-3499, p. 66, ff.

Previous measurements include an extensive set by the Oxford group⁴⁻⁷ using the Harwell syncrocyclotron. A single NaI(Tl) crystal spectrometer was used to study the gamma-ray spectra obtained with targets ranging from ⁶Li to Ca. Unresolved backgrounds were ascribed to neutron effects, and cross sections of typically a few mb were determined for specified gamma-ray energies. From the measured inelastic scattering cross sections, deductions were made concerning the matrix elements for electric multi-pole radiative transition probabilities. Combining the measured gamma-ray yields for levels believed to result from (p,2-nucleon) reactions with results from (p,charged particles) studies led to conclusions concerning the parentages of the ground states in the struck nuclei. Effectively, studies of the gamma-ray transitions provide better energy resolution than charged-particle measurements and thus permit study of the fine structure of the (p,2-nucleon) reactions.

Measurements have been made of the production of bremsstrahlung by protons of 40-185 MeV on Be, C, Al, and Cu (ref. 8). The spectra from these measurements show that the bremsstrahlung contribution extends to higher gamma-ray energies than that from nuclear de-excitation, as expected. However, the cross sections are relatively quite small. Photons from π_0 decay are also shown by the same research to be present in small abundance compared with those from nuclear de-excitation.

For the measurements described in this report, the gamma-ray spectrometer requirements were considered to include ascertainable absolute efficiency, high-neutron rejection efficiency, and an adequate response function (peak-to-total ratio). Multiple-crystal spectrometers were chosen in spite of their attendant complexities and requirement for experimental efficiency calibration. A three-crystal pair spectrometer was used above ~ 2.0 MeV

-
4. A. B. Clegg *et al.*, Proc. Phys. Soc. 78, 681 (1961).
 5. K. J. Foley *et al.*, Nucl. Phys. 31, 43 (1962).
 6. K. J. Foley *et al.*, Nucl. Phys. 37, 23 (1962).
 7. G. L. Salmon *et al.*, Nucl. Phys. 41, 364 (1963).
 8. D. Cohen, B. J. Moyer, H. C. Shaw, and C. N. Waddell, Phys. Rev. 130, 1505 (1963).

and an anticoincidence spectrometer below 2.5 MeV in order to meet the last two requirements. In addition, a time-of-flight requirement was established in order to discriminate against neutron-induced effects. Extensive calibrations of the spectrometer systems were required and are described later.

The results are presented as approximations to the actual gamma-ray distributions produced in the target. This presentation includes correction of the data for the nonunique response of the gamma-ray spectrometer (the so-called spectrum unscrambling) for which a new method due to Burrus was used.⁹

Finally, cross sections for the production of gamma rays of specified energy were calculated wherever peaks in the spectral distributions were sufficiently defined to allow the determination of their areas. These cross sections are compared with those obtained by the Oxford group.

II. Apparatus

A. Gamma-Ray Spectrometer

The choice of a suitable gamma-ray spectrometer is, of course, strongly dependent upon the particular experiment in which it is to be employed. For this experiment the spectrometer had to have reasonable resolution combined with a good peak-to-total ratio, so that gamma-ray lines could be separated; it had to operate in a high-energy neutron field, which required either good neutron shielding or an electronic reduction of the counts due to neutrons in the detector; it had to be fairly compact due to space limitations; it had to be movable to permit measurements at different angles; and finally, a reasonable efficiency was desirable to reduce the required counting time.

The requirement that the spectrometer have reasonably good resolution (where we define resolution as the ratio of the full width at half-maximum of a single peak, expressed in channels, to the channel number of the center of the peak, and reasonably good as 10-15%) led immediately to

9. W. R. Burrus, Neutron Phys. Div. Ann. Progr. Rept., Aug. 1, 1963, ORNL-3499, p. 120.

the consideration of NaI(Tl) detectors. It was expected that gamma rays having energies up to about 10 MeV might be present in significant quantities. To obtain large peak-to-total ratios (which we define as the ratio of the area of the pulse-height distribution under the full-energy peak to the total area under the curve) one must choose either a large (i.e., 5-in. x 5-in. or larger) single crystal, or a multicrystal spectrometer.

There are advantages to each of these types of spectrometers, as there are also disadvantages. A single large crystal has a very much higher counting efficiency than a multicrystal spectrometer. This is desirable since it reduces the cyclotron time required for the experiment. Further, the electronics associated with a single-crystal spectrometer are considerably simpler than those for a multicrystal one. This leads to a cost savings in initial acquisition, reduces maintenance requirements, and lowers the probability of down time due to equipment failure.

The most serious disadvantage of a single-crystal spectrometer is its lack of neutron rejection. In the initial estimates it was assumed that the neutron flux would be equal to the gamma flux, which would result in a prohibitively large background correction. Added to this must be the background due to neutron activation of the large volume of the detector which would result in a very high count rate with correspondingly high count losses. An attempt to reduce the neutron background by shielding the detector would result in a spectrometer far too bulky to move. On the other hand, a multicrystal spectrometer is relatively insensitive to neutrons because of the requirements for accepting an event. Background due to activation of the crystal is kept down because fairly small crystals can be used.

On the basis of these considerations it was decided to use a three-crystal spectrometer. A sketch of this instrument is shown in Fig. 1. Gamma rays to be investigated pass through a collimator into the center crystal ("A" crystal). Here they can interact, giving rise to either a photoelectron, or a Compton electron and scattered gamma ray, or a positron-electron pair. The side crystals ("B" and "C" crystals) are used to determine the type of event which occurred in the A crystal by detecting any scattered photons or annihilation radiation from positron capture. It

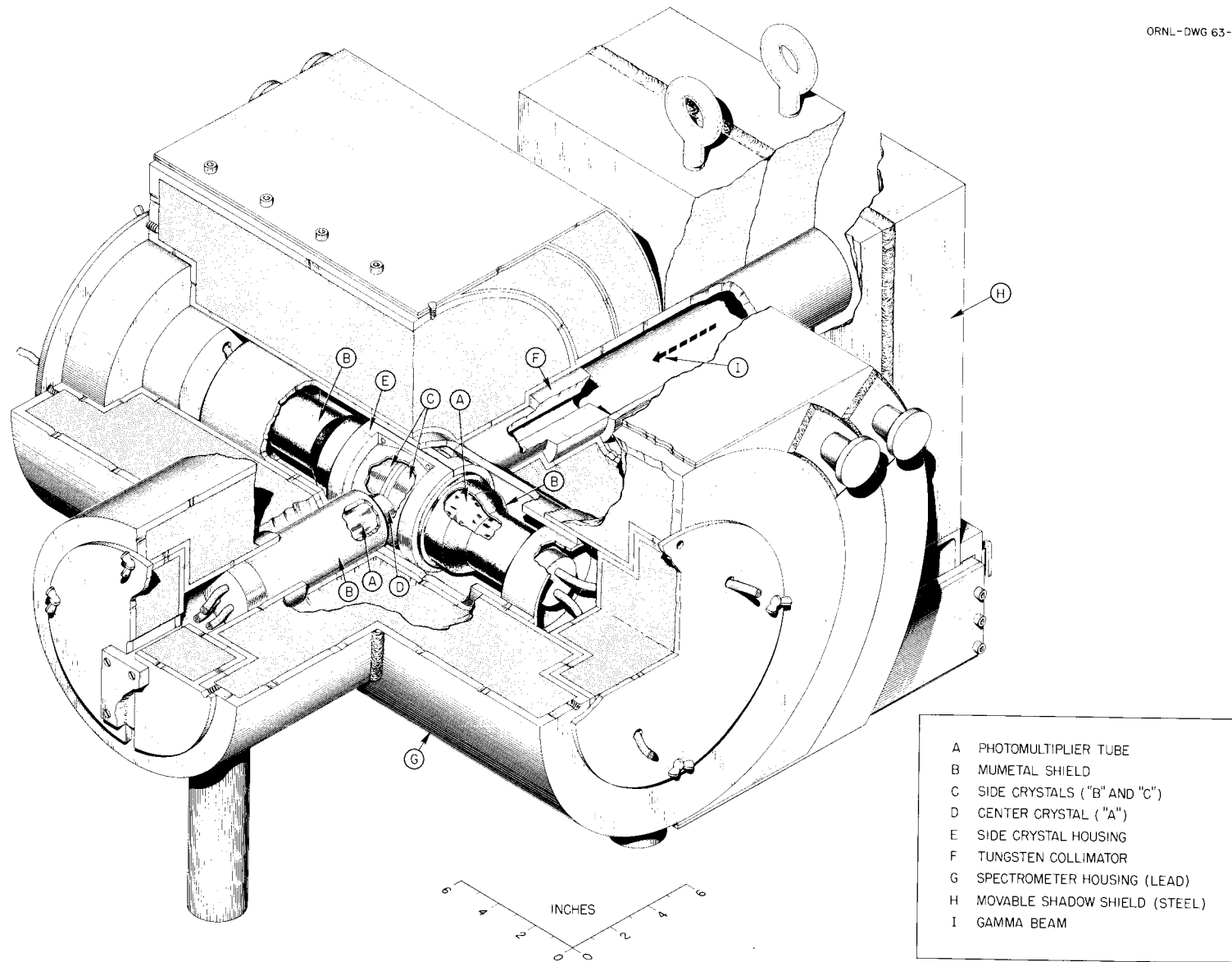


Fig. 1. Three-Crystal Spectrometer Assembly and Housing.

follows that for greatest effectiveness the side crystals should surround the center crystal to the maximum extent possible.

The side crystal assembly designed for this spectrometer is shown in Fig. 2. It consists of two NaI(Tl) crystals in the shape of truncated cones, tapering from 4 in. in diameter to 3 in. in diameter, and 1.872 in. high. A semicylindrical, 1.789-in.-diam groove is cut into the large face along a diameter, so that a cylindrical hole into which the center crystal is placed extends through the assembly. The two side crystals are optically decoupled from each other. DuMont photomultipliers, type 6363, are attached as shown. The solid angle fraction subtended by the side crystals at the center of the hole through the assembly is ~ 0.88 .

The center crystal in this spectrometer is a 1.325-in.-diameter by 1.50 -in.-long NaI(Tl) crystal canned integrally with a 1.325-in.-diameter by 1.75-in.-long NaI light piper. The crystal is mounted on a 56 AVP photomultiplier tube.

The spectrometer can be operated as a pair spectrometer, or as an anticoincidence total-absorption instrument. For the former mode, which was used for gamma rays from ~ 2.0 MeV to 11 MeV, the output of each side crystal within ± 100 keV of the annihilation peak (i.e., 511 keV) was required to be in time coincidence with the output of the center crystal; for the latter mode, the output of the side crystals above ~ 210 keV had to be in anticoincidence with the output of the center crystal. A more detailed discussion will be given later.

While the requirements for accepting an event in this spectrometer are quite stringent, it is yet necessary to provide shielding around the crystals to reduce the background due to random counts occurring in the crystals at the same time. The spectrometer housing shown in Fig. 3 provides a minimum lead thickness of 4 in. around the crystals, increasing to 10 in. of lead at the collimator. An additional 8-in.-thick iron slab, movable to provide easy access to the collimator plugs, is also shown.

-
10. The authors wish to acknowledge the cooperation of the Harshaw Chemical Company in the design and fabrication of this assembly.

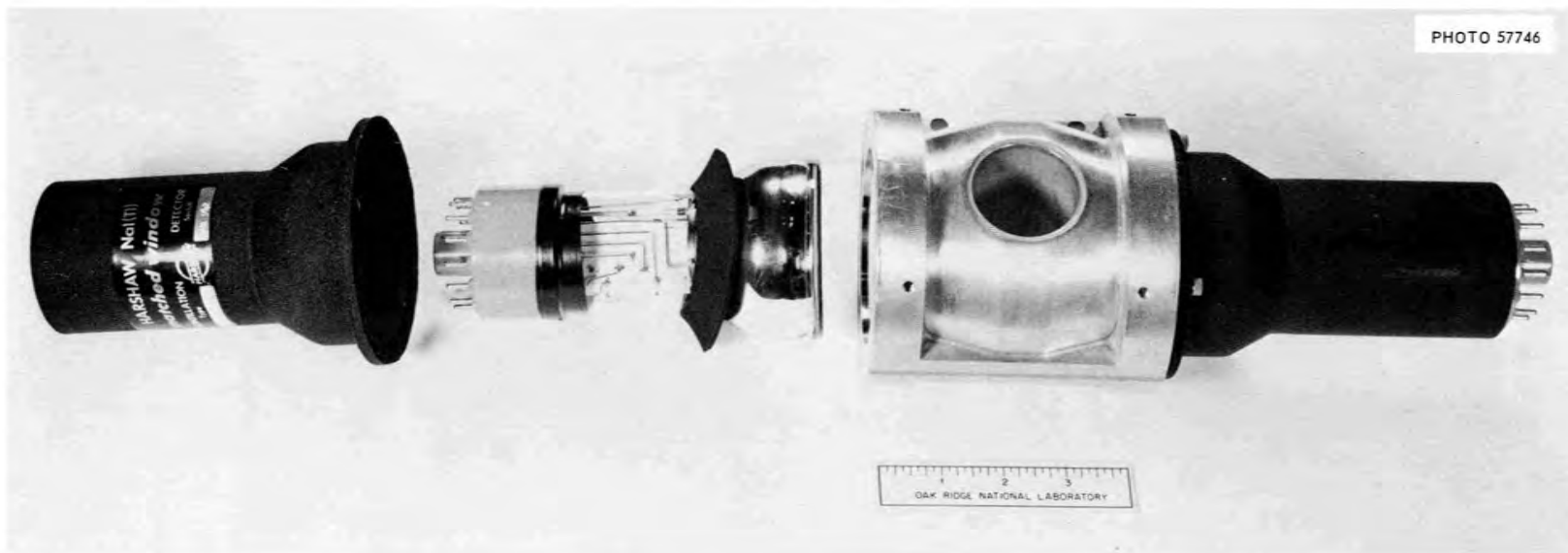


Fig. 2. Assembly of Side Crystals and Photomultipliers.

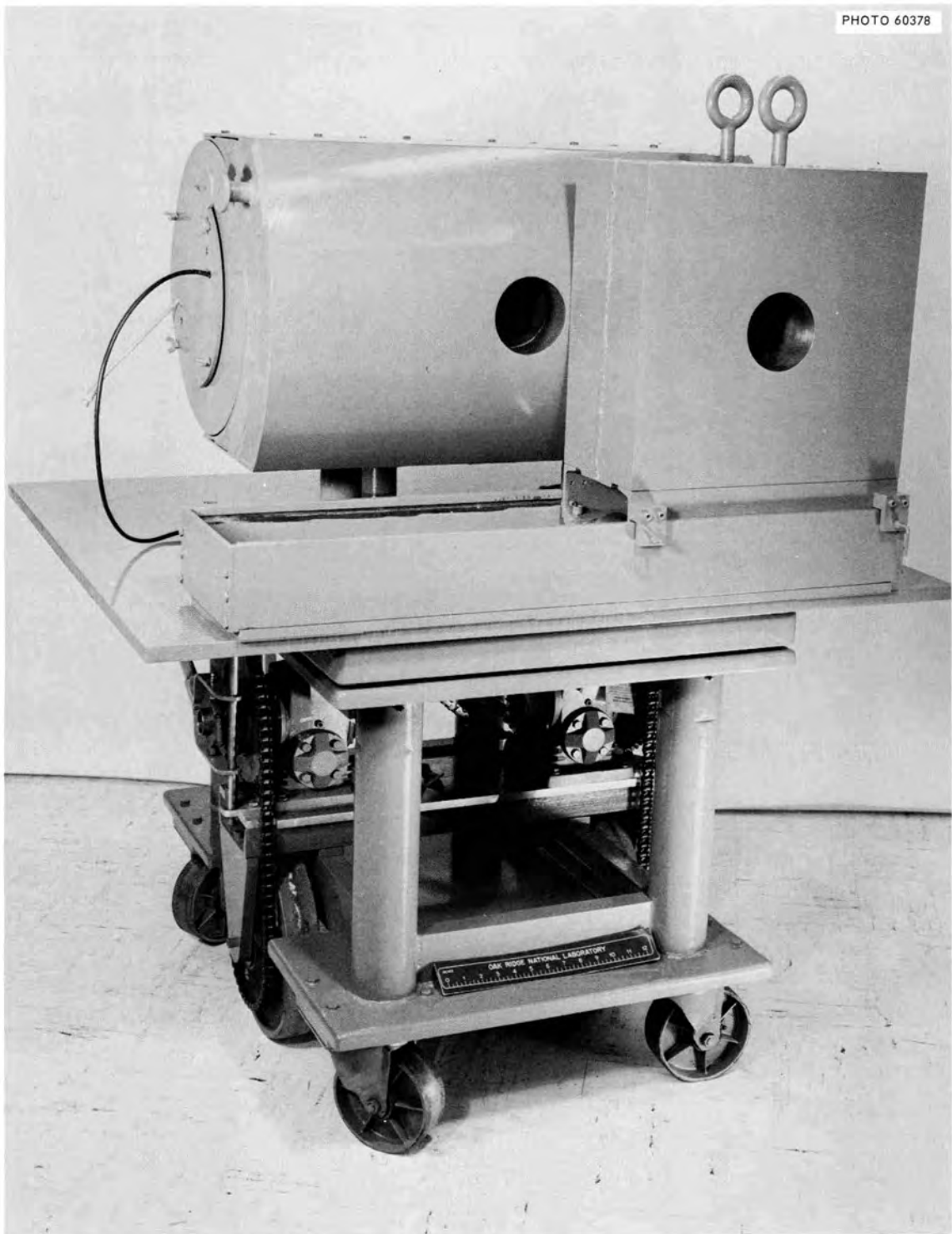


Fig. 3. Spectrometer Shield and Movable Support.

The collimator plugs, nominally 6-15/16-in. long, are made of a wolfram alloy¹¹ containing 92.5 wt% W, 4.5 wt% Ni, and 3.0 wt% Cu, with a density of $\sim 17.6 \text{ g/cm}^3$. The collimator was a 3/4-in.-diam straight hole through the plug. A similar plug, but without the hole, was available to measure background radiation. Also used in this experiment was a tapered collimator, designed to accept radiation from a 6-cm-diam source at a distance of 70 cm between the center of the A crystal and the source disk.

B. Neutron Rejection by Time of Flight

As pointed out above, a multicrystal spectrometer is rather insensitive to incident neutrons. Early checkout runs indicated a rather large background, however, which could be ascribed to the neutron field. It was therefore decided to attempt a reduction of this background by a time-of-flight method of neutron rejection.

Since the proton source is a synchrocyclotron, the proton beam is not continuous in time but is confined to an interval of time, or "macroburst," which depends upon the machine parameters. Within each macroburst exists a fine structure due to the rf acceleration of the protons, which gives rise to "microbursts." The proton beam therefore arrives at the target in discrete bunches.

The time at which the neutrons and gamma rays start from the target is determined from the arrival time of each proton bunch. The neutrons have all energies up to a maximum given by the proton energy and the angle of emergence. The maximum neutron speed is considerably less than the speed of the gamma rays. The spectrometer is arranged so that only those events are recorded which are detected at a time after the arrival of the proton bunch at the target equal to the flight time of the gamma rays. Since the proton microburst is spread over a finite time (in this case $\sim 5 \text{ nsec}$ full width at half maximum), events must be accepted within this time interval.

If there were just one microburst, the effect of the neutron field would be removed and a large single-crystal spectrometer could be used. In

11. Supplied by the Kulite Tungsten Company, 1040 Hoyt Avenue, Richfield, N. J.

practice, however, there are many such microbursts, separated within a macroburst by a time depending on the rf frequency of the accelerating field at the time of beam extraction. It follows that the effect of the fastest neutrons will be eliminated but not that due to the slower neutrons which arrive just when the spectrometer is ready to accept the gamma rays from the next microburst. Although the improvement will depend upon the neutron spectrum, one can expect to reduce the neutron-induced background roughly by the ratio of the length of a microburst to that of one rf cycle. The rejection achieved will be discussed later in more detail.

To determine the arrival of the protons at the target two methods were considered. The first is to sample the cyclotron rf accelerating voltage and derive a timing signal from it. A more direct method is to place a parasitic scintillation detector in the proton beam before the primary particles strike the target. The latter scheme was used in this experiment. A thin (2-mm-thick) organic scintillator* mounted on a 56 AVP photomultiplier and covered with 0.005-in.-thick aluminum foil was used as the detector. The energy loss per proton traversing the detector (also called the D scintillator) was ~ 930 keV.

Figure 4 shows the functional block diagram of the timing circuitry. The variable delay, T_1 , is necessary to compensate for the difference in the signal transmission time from the A and D scintillators, respectively, to the prompt coincidence circuit input. The A detector signal from the NaI(Tl) crystal is taken from the anode of the 56 AVP photomultiplier and fed into a 125- Ω RG-63 clipping line and transmission line. This signal is referred to as A*. Care was taken to reduce stray capacitance at the photomultiplier anode in order to preserve the rise time of the anode current pulse. The 13-nsec clipping line is necessary to prevent double-pulsing in the prompt coincidence circuit due to the slowly decaying portion of the anode current pulse. The anode current pulse of the D scintillator has a total decay time (4τ) of ~ 16 nsec, therefore no double-pulsing can occur for a pulse separation of ~ 40 nsec.

*Spectrum Plastic Scintillator, manufactured by Semi-Elements, Inc., Saxonburg, Pennsylvania.

ORNL-DWG 64-8053

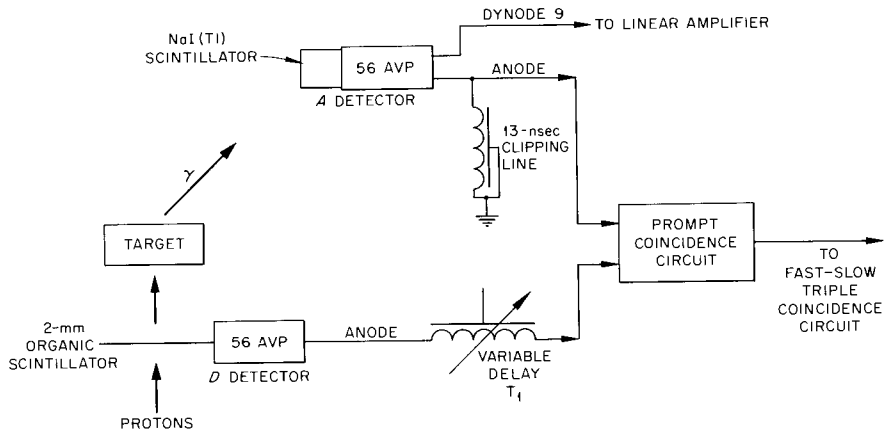


Fig. 4. Functional Block Diagram of Timing Circuit.

The prompt coincidence unit takes advantage of the very fast switching speed of tunnel diodes to detect the coincidence of events at the A and D detectors.¹²⁻¹⁴ The schematic diagram is shown in Fig. 5. As Fig. 5 shows, the prompt coincidence unit is designed around one basic univibrator circuit. This particular circuit has been described in detail elsewhere;¹⁵ therefore only its performance will be described here.

One very important aspect of any circuit used for timing applications is propagation delay, defined as the time delay between the arrival of a signal and the occurrence of the output signal. The change in propagation delay with various input amplitudes is commonly called "walk." With careful circuit layout techniques the walk of this basic circuit can be held to about 2 to 3 nsec for an order of magnitude change in the input signal when the initial trigger magnitude is set 30% above the minimum trigger threshold.

The lower level discrimination and limiter action for the coincidence unit is performed by tunnel diodes TD_1 and TD_5 for the A and D channels, respectively (see Fig. 5). The tunnel diode TD_1 is constant-current-biased in its low-voltage state by the current-limiting resistors, R_3 and R_4 , to a value of about 8.5 mA. When the summation of the bias current and the photomultiplier anode current exceeds the tunnel diode peak current (10 mA), the tunnel diode will switch to its high-voltage state and thereby generate a standardized output pulse. The width of the output pulse is determined by L and R_L and is the time necessary for the tunnel diode to relax back to its stable, quiescent, low-voltage condition.

The incoming signals to both the A* and D input have a wide dynamic range of values. The A channel, for example, can accommodate a factor of 20 in its linear output presentation to the analyzer. The pulse height of the D input signal varied according to the number of protons in each

-
12. A. Whetstone and S. Kounosu, Rev. Sci. Instr. 33, No. 4, 423 (1962).
 13. R. H. Bergman, M. Cooperman, and H. Ur, RCA Review, p. 152 (June 1962).
 14. S. Gorodetsky, Nucl. Instr. and Methods 14, 205 (1961).
 15. N. W. Hill et al., Apollo Instrumentation, ORNL-TM-615 (to be published).

ORNL-DWG 64-8052

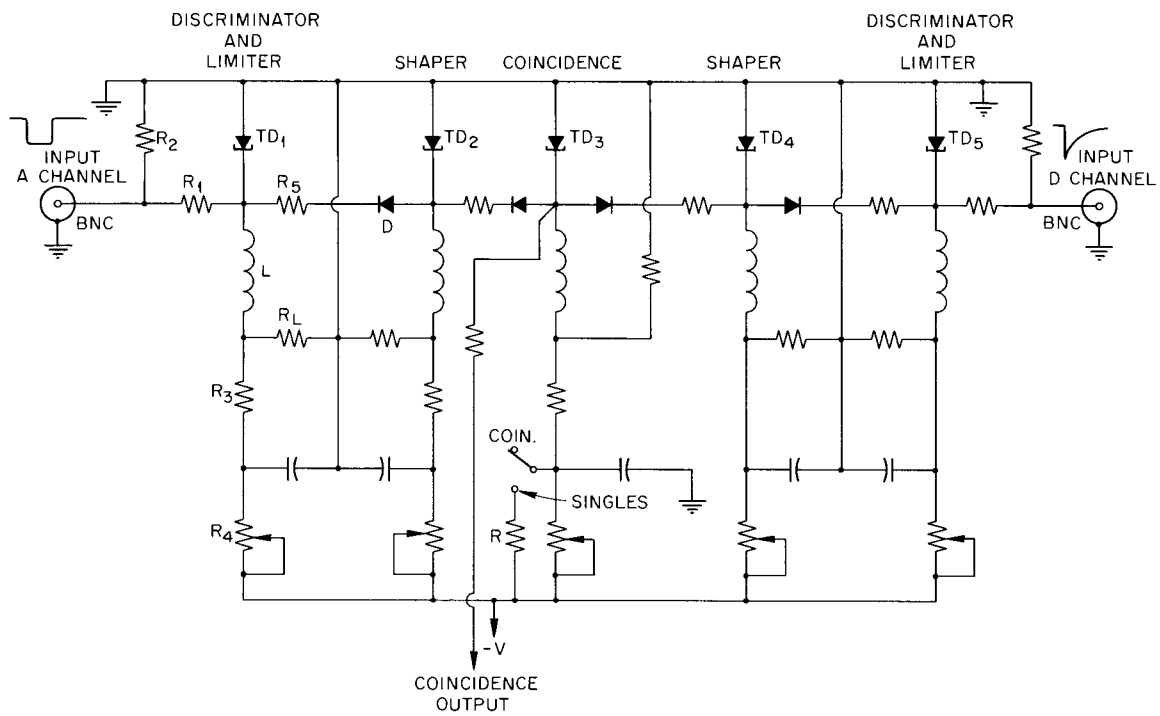


Fig. 5. Schematic Diagram of Fast Coincidence Circuit.

microburst of the proton beam.¹⁶ The limiter tunnel diode, TD₁, has an output voltage vs input voltage slope of approximately 1/30 for inputs exceeding the limiter trigger threshold. For severe overdrive, i.e., a factor of 100, the slope increases to about 1/20. The output pulse width of the limiter is also slightly dependent on the degree of overdrive. To make the A* and D shaped inputs into the coincidence diode TD₃ insensitive to the amplitude of the respective inputs, an identical shaper circuit was interposed between the limiter and coincidence diode. The signals going into TD₃ had an effective output to input slope of about 1/600 referred to the input. This results in very good protection from "singles feed-through." To allow only one input to trigger the coincidence circuit, it was necessary only to raise the bias current in TD₃ by operation of a switch.

Figure 6 shows representative resolution time curves for the coincidence unit, as obtained with a fast pulser. The two curves were taken with a fixed value of inductance but with different values of bias current in the coincidence tunnel diode. A reasonable change in resolution time can be accomplished by simply changing the bias current. The input pulses used to obtain the data of Fig. 6 had a full width at half maximum of 5 nsec for channel A and 7 nsec for channel D.

C. Discussion of Electronics Block Diagram

The electronic circuitry necessary for this spectrometer is dictated by the particular mode of operation, i.e., pair spectrometer or total absorption spectrometer. The pair spectrometer requires that the outputs of the B and C channels correspond to (511 ± 100) keV, and that they be in time coincidence with an output corresponding to more than approximately 500 keV deposited in the A crystal. The total absorption spectrometer requires the output of the A channel to be in anticoincidence with an output corresponding to more than ~ 210 keV deposited in either of the side crystals. One final requirement on both operating modes is imposed by

16. R. T. Santoro, et al., The Space, Time, and Energy Distribution of the Proton Beam of the Harvard University Synchrocyclotron, ORNL-3722 (1965).

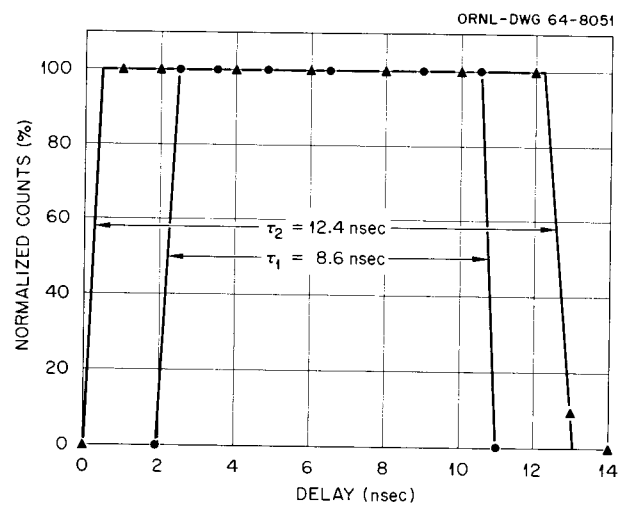


Fig. 6. Delayed Coincidence Curves Obtained with a Pulser for Different Bias Levels of the Discriminator in the Fast Coincidence Circuit.

demanding that the spectrum taken in A be in time coincidence with the proton beam striking the target. The block diagram of the spectrometer for both pair and total absorption modes is shown in Fig. 7. It is seen from the diagram that the same basic instruments are used in both modes of operation and to change from one mode to the other only involves only some minor cable rerouting and switch settings. All of the individual instruments shown in the block diagram will be discussed below.

Scintillation Detectors. The fast timing signal for use in neutron rejection as discussed above was generated in a 2-mm-thick organic scintillator used as a beam detector. The crystal was mounted on a 56 AVP photomultiplier with a bleeder string layout specially designed¹⁷ to minimize the anode current rise time. A typical value for the rise time is 3.2 nsec for a current pulse of 55 mA into a 50- Ω load. Figure 8 shows the schematic of the voltage divider.

The performance of a NaI(Tl) scintillation spectrometer is limited in general by the scintillation crystal and its accompanying photomultiplier tube. The primary criterion is generally considered to be the photopeak resolution which is usually determined from the width of a Cs¹³⁷ photopeak as displayed on a multichannel analyzer. This criterion had to be compromised in this experiment due to the demand of the fast timing circuit for a current that could be taken directly from the photomultiplier anode. Several ten stage 1-1/2-in.-diameter tubes were tested against the above criteria but none were found to furnish sufficient anode current at the lower energy levels, i.e., at 200 keV. A 56 AVP was selected as the type that satisfied the requirement listed and also exhibited gain shifts with counting rate changes that were small enough to be tolerated. The tube and crystal combination used in this experiment has a resolution (full width at half maximum) of 12.2% for the Cs¹³⁷ gamma ray at a counting rate of 920 cts/sec. Figure 9 shows the voltage divider network of the A tube and the divider for both the B and C tubes is shown in Fig. 10.

High-Voltage Power Supplies. The current gain of a photomultiplier is proportional to approximately the seventh power of the applied voltage.

17. The layout was designed by E. E. Waugh, ORNL Instrumentation and Controls Division.

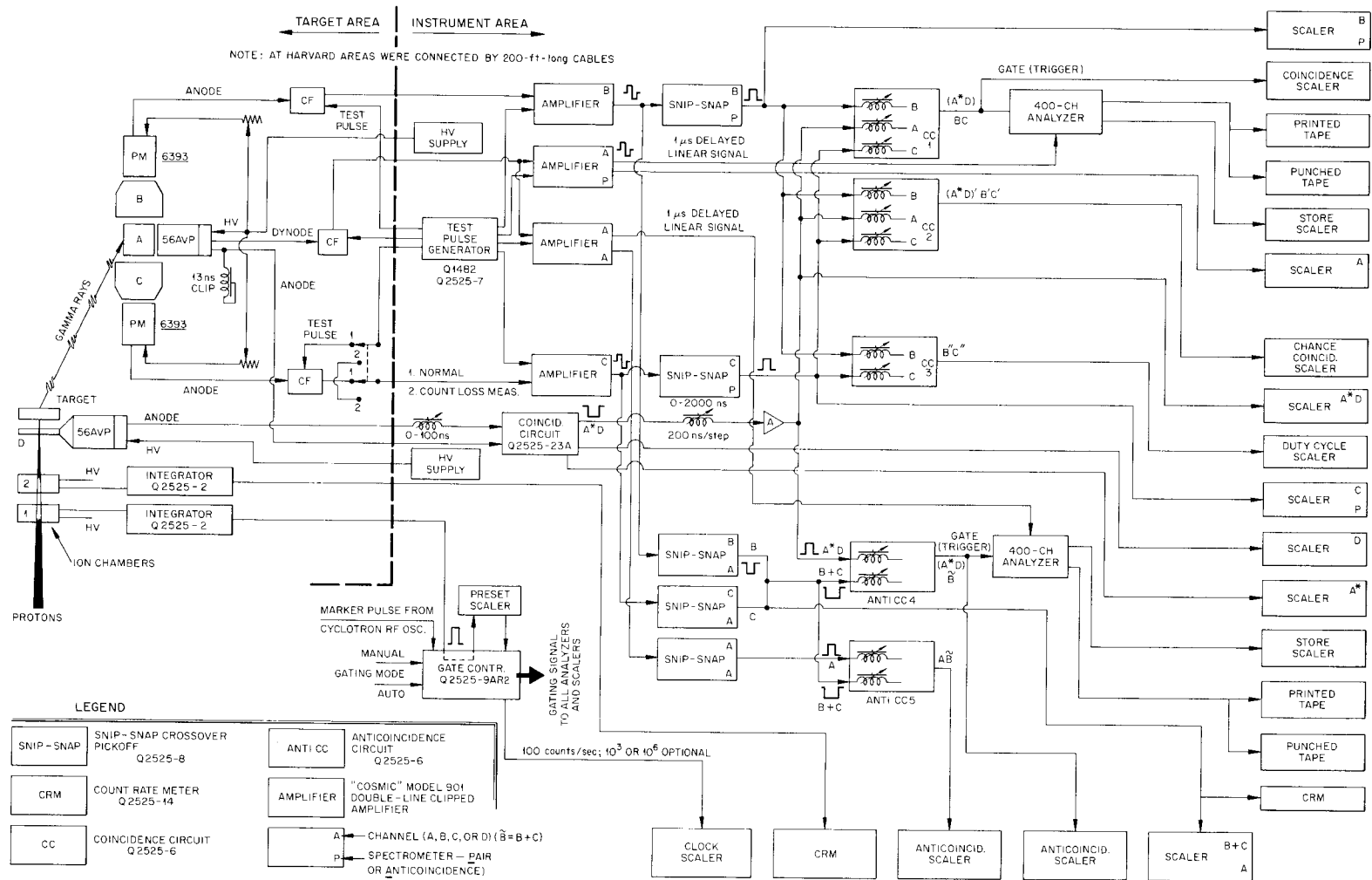


Fig. 7. Block Diagram of the Spectrometer Electronics for Both Pair and Total Absorption Modes.

ORNL-DWG 64-8048

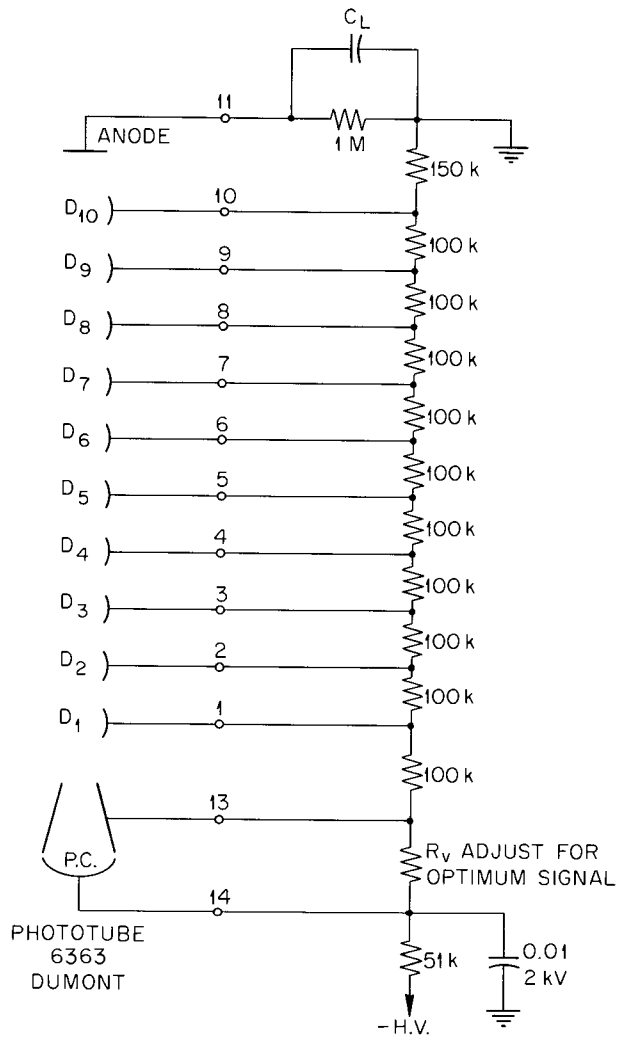


Fig. 10. Voltage Divider for Type 6363 Photomultiplier Used with "B" and "C" Detectors.

Therefore the gain stability of the spectrometer is critically dependent upon the stability of the high-voltage power supplied to it.

Two high-voltage supplies were used in this experiment. A separate supply for the D tube was desirable since the high voltage had to be adjusted for different beam intensities to prevent the D tube from going into current saturation. The D supply was a John Fluke Model 408A with an output of 500-6000V at 0-20 mA. The supply for the three tubes comprising the spectrometer was a John Fluke Model 405 with an output of 600-3100V at 0-15 mA. The output from the supply was fed directly to the A tube and was nominally 1850 volts. A resistance divider string dropped this voltage to approximately 800 volts for the side channel photomultipliers. Tests on these power supplies under actual operating conditions have shown the voltage stability to be better than 0.1%.

Test Pulse Generator. A four-channel precision test pulse generator allowed a shaped pulse to be fed simultaneously into the linear amplifiers or preamplifiers of the various channels. The shape of the test pulse was made to match that of an integrated NaI pulse in order to avoid inconsistencies caused by variations in pulse shape. A generator of this type is necessary for proper alignment of the coincidence circuit, measurement and adjustment of time delays between the various signal channels, as well as for proper testing of the stability and linearity of the analyzer, amplifiers, and preamplifiers. The pulse generator also is used to determine the count losses as described below.

Preamplifiers and Amplifiers. The preamplifiers used in this experiment were Tennelec Inst. Co. Model 022062 White cathode followers. Separate test and detector inputs were provided to allow mixing of the detector signal and the test pulse generator signal. As seen on the block diagram the preamplifier is physically close to the detectors and drives 200 ft of cable to the amplifier input.

The linear amplifiers were Cosmic Radiation Labs., Inc. Model 901 which is based on the design of Chase¹⁸ and uses double-delay-line wave shaping, resulting in a minimum base line shift at high counting rates.

18. R. L. Chase and V. Svelto, IRE Trans. Nucl. Sci., Vol. 8, No. 3, p. 45 (1961).

The amplifiers have sufficient bandwidth to allow a choice of clipping lines to produce output pulse widths between 0.5 μ sec and 4.0 μ sec. Clipping lines producing 0.5- μ sec pulse widths were used in this experiment. The maximum gain of the amplifier is 600. The gain is changed by varying the feedback impedance in the amplifying loops. This method has the unfortunate effect of changing the bandwidth of the amplifier, and a change of the pulse rise time accompanies any change in amplifier gain. Since "zero crossing" is used to perform the coincidence timing following the amplifier, a change in rise time results in a slight change in the zero crossing time. This necessitates checking the coincidence timing after every gain change. The change in zero crossing time with respect to input amplitude changes, or walk, for a given gain is typically 3 nsec for an output voltage change of from 0.5 V to 10 V when measured with the test pulse generator. Both a prompt output and an output delayed by 1 μ sec are available.

Snip-Snap Single-Channel Analyzer. The snip-snap single-channel analyzer¹⁹ acts as a zero crossover pick-off and pulse shaper which drives the coincidence circuit. The power supply in the linear amplifier furnishes the power for the snip-snap chassis. The single-channel analysis consists of a lower discriminator and an upper discriminator, whose outputs are in anticoincidence. When an input pulse triggers the lower discriminator, a feedback scheme which is incorporated in the discriminator level control changes the discriminator hysteresis so that the discriminator returns to the normal state as the input pulse crosses over zero volts. A pulse is generated when crossover is detected and is delivered to the output unless the upper level discriminator is triggered, which inhibits the pulse before it reaches the output. Both the lower and upper discriminators are adjustable over 0 to 10 V. The output pulse amplitude is 6 V and rise time is typically 20 nsec. A typical value of the walk is 5 nsec for a 0.1- μ sec rise time input pulse varied from 0.5 V to 10.0 V in amplitude. The upper level discriminator can be made inoperative by simple switch action. The circuit diagram is shown in Fig. 11.

19. Described by T. L. Emmer in ORNL-TM-137 and shown in ORNL I and C Div. Dwg. Q-2525-8.

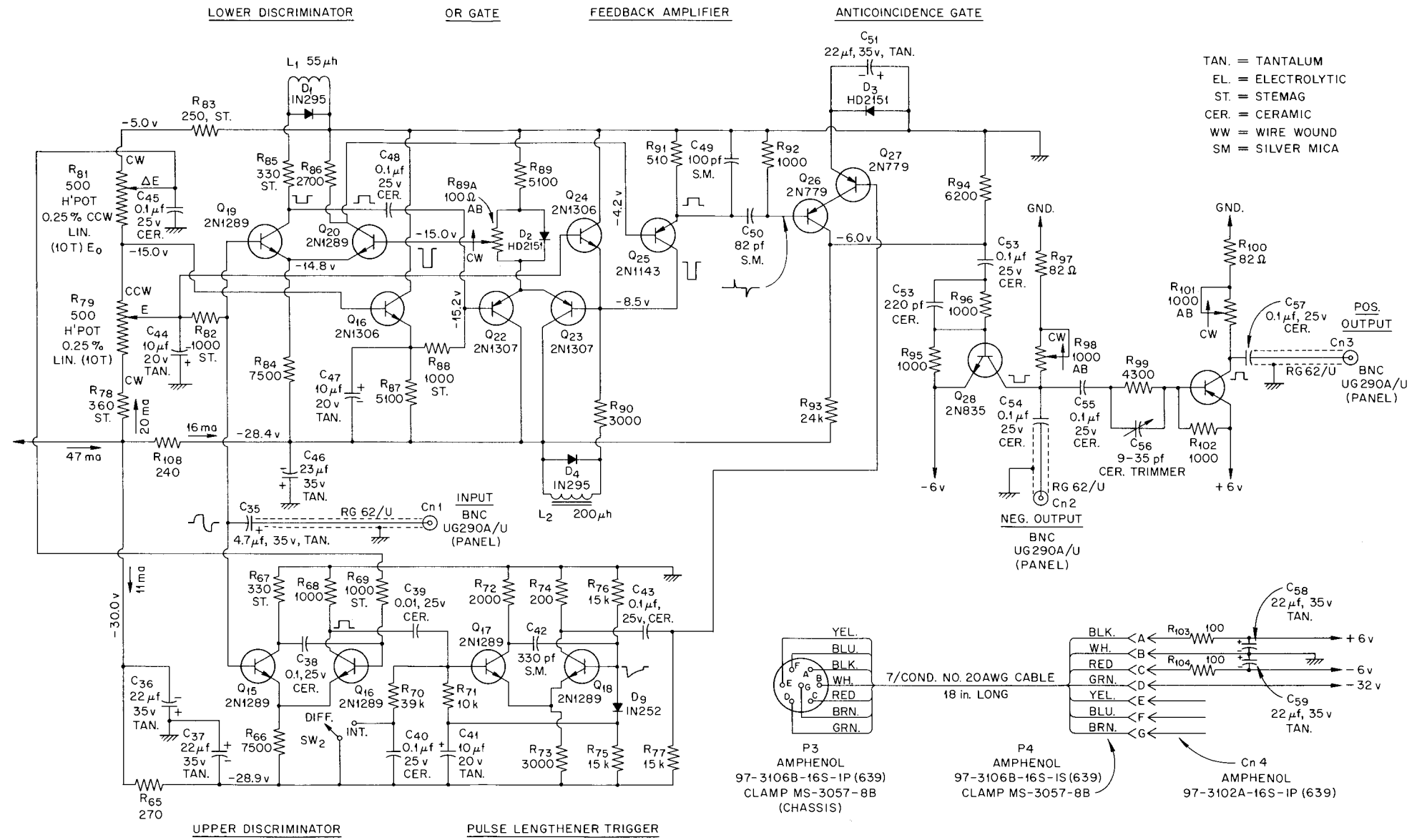


Fig. 11. Schematic Diagram of Snip-Snap Single-Channel Analyzer and Cross-Over Pick-Off Circuit.

Coincidence Circuit. The snip-snaps in channel B and C determine the energy deposited in the side crystals and send an input to the coincidence circuit²⁰ to determine the time coincidence of selected events. The A*D coincidence determines the proper timing of events in A with respect to the proton beam and generates a signal input to the coincidence unit which is placed in triple coincidence with selected events in B and C. So that rapid adjustments of the timing of these events can be made, 250-nsec, 20-turn delay lines (Helidels²¹) are incorporated on the three separate inputs. Also, as an aid to alignment, switches allow rapid changes from one mode to another, e.g., from a three-fold coincidence to a two-fold or one-fold coincidence, from a two-fold coincidence to a two-fold coincidence and one anticoincidence, etc.

The resolution time of the circuit is controlled by miniature coaxial cables used as shorted delay lines. Clipping times of 25 nsec were used on the B and C inputs and 40 nsec was used on the A*D input. The anti-coincidence input was clipped at 80 nsec. Figure 12 shows the schematic diagram.

Pulse-Height Analyzer. The analyzer used in this experiment was an RIDL Model 34-12. Auxiliary output equipment included a Tally paper tape punch and a Hewlett-Packard paper tape printer.

Count-Rate Meter. Monitoring of the count rate in the A channel and of the proton beam intensity was performed with the aid of a linear count rate meter.²² The rate meter has separate positive and negative inputs with integral discriminators variable from 0.5 V to 10.0 V. The instrument has a five-decade counting range with 100,000 cps being the maximum average counting rate. Input pulse rise time must be faster than 0.75 μ sec and pulse width must be \geq 10 nsec. A remote indicating meter is available and was used extensively during the experiment by the cyclotron operator as a

20. Shown in ORNL Instrumentation and Controls Div. Dwg. Q-2525-6.

21. Helipot Corporation, Newport Beach, California.

22. Designed by J. H. Todd, Instrumentation and Controls Division (ORNL) and shown in ORNL I and C Dwg. Q-2525-14.

convenient method of monitoring the average beam intensity. An integrating time constant can be chosen from 10, 1, or 0.5 sec values. A range multiplier is provided which multiplies any range by 0.25, 0.5, or 1.0. A scale expander allows the indicating meter scale to effectively be expanded or contracted by 40% of full-scale deflection.

Scalers. All scalers used in this experiment were obtained from commercial vendors. The preset scaler was a CMC Model 786C modified in our laboratory so that it could be remotely controlled by the gate control circuit. The remainder of the scalers were Transistor Specialties, Inc. Model 1511 with modified readout to include a four-digit register in addition to the seven Nixie digits normally provided.

D. Beam Monitor and Control Circuit

In order to normalize the data with respect to the proton beam intensity, a beam monitoring system was used.²³ The system consists basically of a specially designed ion chamber and ion current integrating electrometer. The current integrator translates the d-c ion current into a voltage pulse, where one voltage pulse is generated per unit charge collected. This monitoring system allows the experimental data to be collected in an easily controlled manner.

Data collection is controlled by gate control circuit.²⁴ A block diagram of the instrument is shown in Fig. 13. Briefly, the instrument works as follows: the ion current is continuously integrated, and a voltage pulse is generated per unit charge accumulated. The complete data-acquisition system, as shown in the pair and total-absorption spectrometer block diagrams, is gated ON immediately upon the generation of the first voltage pulse after the manual START button has been pressed. All data acquisition equipment is gated simultaneously and remains ON until a preset number of unit charges have been collected by the ion chamber. Upon reaching the preset total charge accumulation, the gate control circuit turns OFF all data-acquisition equipment simultaneously.

23. R. T. Santoro and R. W. Peelle, Measurement of the Intensity of the Proton Beam of the Harvard University Synchrocyclotron for Energy-Spectral Measurements of Nuclear Secondaries, ORNL-3505 (March 1964).

2-01-058-800A

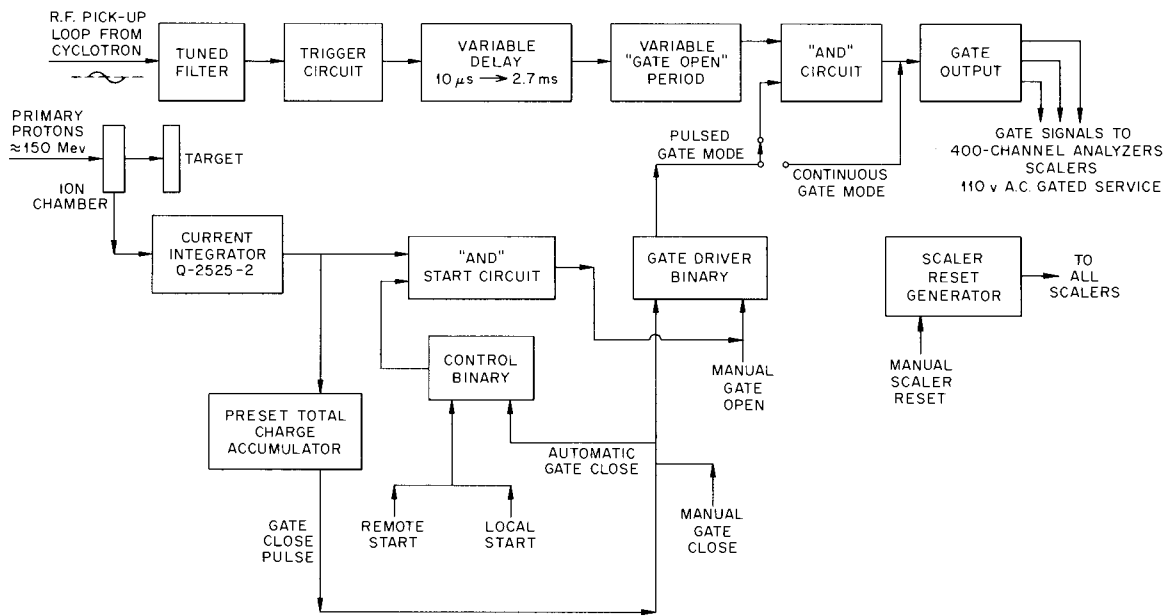


Fig. 13. Block Diagram of Gate Control Circuit.

Since a high background was present, the gating system was designed so that it could alternately be used to gate ON only during selected portions of the beam period. The sampling interval could be varied from 100 to 400 μ sec in width and could be selected to occur at any given location in the beam period. This sampling flexibility allowed gating to be selected over the macrostructure, over the background, or during a composite time interval containing both macrostructure and background.

E. Target Description

The choice of target materials was influenced by the materials of interest to the APOLLO program at the time. Since it was felt to be impractical to measure all materials, representative light, medium, and heavy elements were chosen for comparison with possible theoretical studies. For the latter reason monoisotopic substances were desirable. As the materials had to be available in rather large quantities, formable into the proper shapes, and of reasonable cost, the choice of the final list was almost inevitable.

The thickness of the chosen targets was a compromise between yield, which requires many interactions and therefore a thick target, definition of the gamma-ray origin, which ideally should be a point, i.e., a very thin target, and minimal self-absorption of the emitted gamma rays in the target, which also requires a thin target. In general the choice favored a thicker target to get the necessary intensity. For the lighter elements the targets were nominally 30-MeV thick, and for the heavier elements, Co and Bi, the nominal target thickness was 11 MeV.

In determining the useful energy range of the spectrometer it was felt that the ^{128}I gamma-ray activity (0.428 MeV) would make attempts at measurements below 0.50 MeV rather meaningless. Thus, 0.50 MeV was taken as the lower limit, and the transmission of the targets for gamma rays of this energy was calculated as representing the least favorable case. Since most of the measurements were made at 136° , the calculations were made at this angle. The average transmission for 0.50-MeV gammas at 136° varied from 66% for Bi to 84% for Co, with the lighter elements varying from 69% for Al to 74% for Be. From intensity considerations it was felt that the target thicknesses noted above should not be reduced.

The targets used in this experiment are listed in Table 1.

F. Disposition at Synchrocyclotron

The general arrangement of the experiment at the synchrocyclotron is shown in Fig. 14. The Harvard University 95-in. synchrocyclotron is a frequency-modulated machine producing unpolarized protons at a nominal energy of 160 MeV, with an energy spread of about 2 MeV and fluxes as high as 5×10^{10} protons/sec. Its frequency ranges from 23-30 Mc/sec, modulated by a rotating condenser. The nominal beam area is 7 cm^2 or less. The permanent shield consists of from 3 to 8 ft of ordinary concrete.

Table 1. Targets

Material	Diameter (cm)	Thickness (g/cm ²)	Energy Loss in Target (MeV)
Be	7.6	6.055 ± 0.030	27.4 ± 1.2^a ± 1.6
C	7.6	6.002 ± 0.030	30.1 ± 1.4^a
H ₂ O	7.6	5.10 ± 0.05	30.0 ± 2^b
Al	7.6	6.808 ± 0.034	29.1 ± 1.1^a ± 1.6
Al	20.0	26.715 ± 0.16	159 ± 2^c
Co	7.6	3.224 ± 0.016	11.16 ± 0.56 ^{0d}
Bi	7.6	4.505 ± 0.023	11.36 ± 0.11^e

- a. Calculated from difference in range, using linear interpolation of data given by R. M. Sternheimer, Phys. Rev. 115, 137 (1959).
- b. Calculated from difference in range, using curves by M. Rich and R. Madey, UCRL-2301 (1954).
- c. The target thickness is greater than the range of the incident protons.
- d. Calculated using $dE/\rho dx$ data of Sternheimer for Cu.
- e. Calculated using $dE/\rho dx$ data of Sternheimer for Pb.

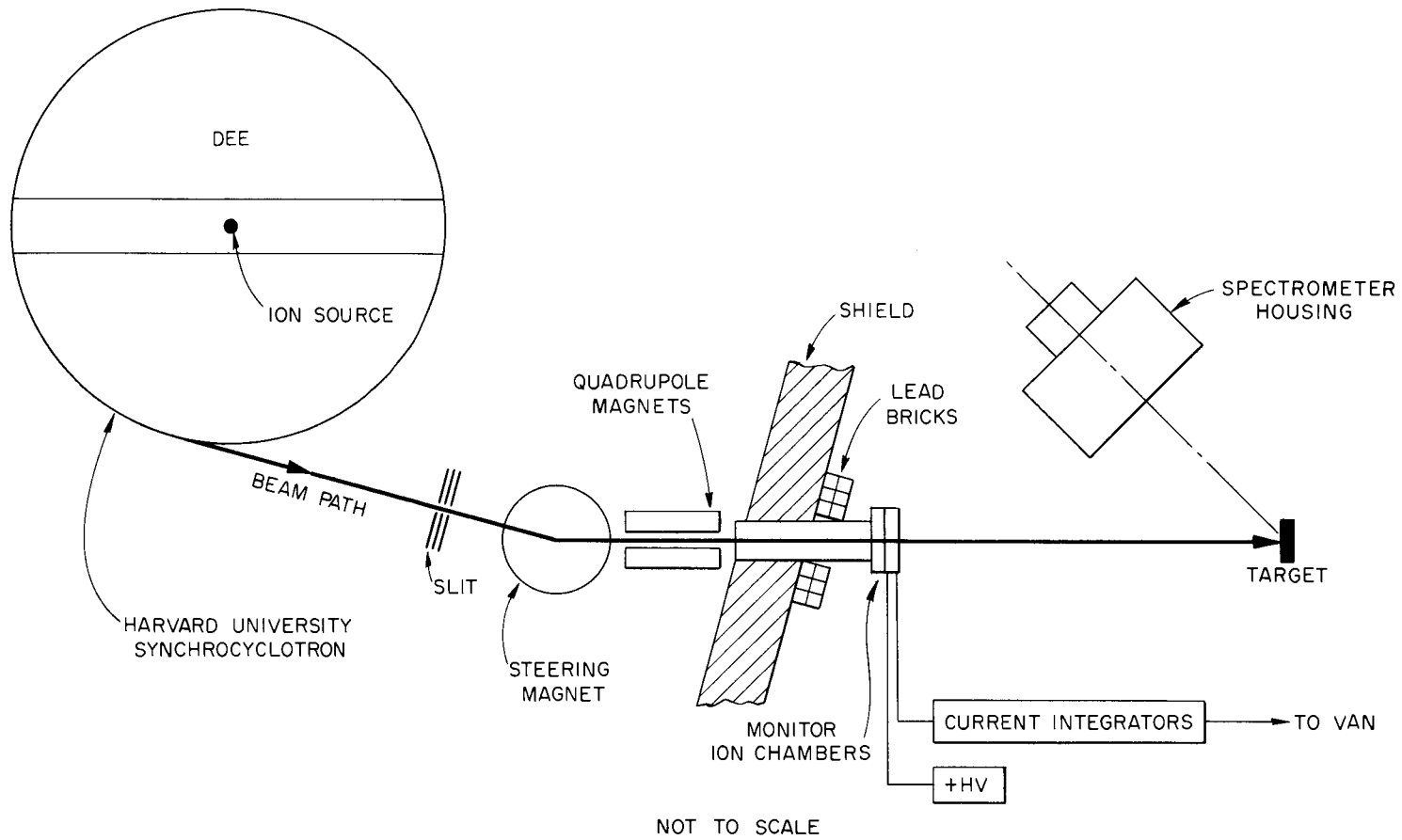


Fig. 14. General Arrangement of the Experiment at the Harvard Synchrocyclotron.

The proton beam emerging from the machine passed through a system of slits before being deflected by a steering magnet and focused by two quadrupole magnets. The beam continued down a beam tube, passing through two monitoring ion chambers before impinging on the target. Lead bricks were stacked at the exit end of the beam pipe, as shown in the figure, to reduce the background.

The beam was aligned on the target by the use of Polaroid film. A typical picture is shown in Fig. 15. The beam size is approximately $3/4$ by 1 in. The spectrometer was then positioned with respect to the target, using a graduated bar along the centerline of the A crystal to determine the distance, and a protractor at the end of this bar to determine the angle between the beam and the spectrometer axis.

The majority of the measurements were made at a distance between the center of the A crystal and the intersection of the spectrometer axis with the beam of (104.1 ± 0.2) cm, and at an angle of $136^\circ \pm 0.5^\circ$ from the forward beam direction. A limited number of measurements were also made at a distance of (102.8 ± 0.2) cm and an angle of $44^\circ \pm 0.5^\circ$, and at a distance of (155.9 ± 0.2) cm and an angle of $20.5^\circ \pm 0.5^\circ$.

III. Calibrations

A. Gain and Gain Shift with Count Rate

Since it is desired to know the energy of the gamma rays incident on the detector, and the output of the spectrometer was a pulse-height distribution in volts, it is necessary to know the conversion parameters from MeV incident energy to volts recorded. This conversion was obtained from the so-called gain curve.

The gain curve was determined by measuring the pulse-height peak positions, taken with the operating values of photomultiplier high voltage and amplifier gain setting, for radioactive sources having one or two gamma rays of known energy. As there may have been variations with time in the high voltage and/or the amplifier gain it was desirable to check this gain curve for each run.



Fig. 15. Typical Image Produced on Polaroid Film by the Proton Beam at the Target Position.

The calibration sources used in this experiment were ^{22}Na and ^{137}Cs for gain calibration of the anticoincidence spectrometer and ThC'' and Am-Be for the pair spectrometer. For the Am-Be source a 1/4-in.-thick lead filter was required to eliminate the very large number of low-energy gamma rays which otherwise raised the count rate to intolerable levels. The sources and energies of the gamma rays are listed in Table 2.

Table 2. Calibration Sources

Source	Energy of Gamma Ray Used (MeV)
^{22}Na	0.511, 1.27
^{137}Cs	0.662
ThC''	2.62
Am-Be	4.43

It has been observed previously, and again in this experiment, that the apparent gain of a photomultiplier is not only a function of the applied high voltage, but also a function of the count rate. It was therefore necessary to either find a photomultiplier which does not exhibit this gain shift in the counting range of interest, or to calibrate at the count rate applicable to the experiment. Since the latter was difficult to predict it was easier to try to find photomultipliers which would not exhibit this gain shift at the maximum count rates expected.

The shift in the side channels, B and C, was checked at the operating voltage of 840 V with the 0.511-MeV gamma ray of a ^{22}Na source. The gain at ~ 900 cts/sec was taken as the norm, and gain shifts at higher count rates were computed as percentage differences from this gain. The gain in channel B decreased with increasing count rate by as much as 2.8% at ~ 6000 cts/sec, then increased again to reach the original value at ~ 22000 cts/sec, and increased further to an excess of more than 3% over the original value at ~ 81000 cts/sec. Under the same conditions the gain in channel C remained constant until the count rate exceeded ~ 22000 cts/sec, and increased by 1.5% at ~ 81000 cts/sec.

The shift in channel A was investigated as a function of gamma-ray energy as well as of count rate. It was noted that the shift occurred at lower count rates with increasing gamma-ray energy, which might be expected if the shift is due to a photomultiplier tube current phenomenon. For ^{137}Cs and ^{60}Co sources the gain shifted upward, increasing by about 1% at $\sim 50,000$ cts/sec. For ^{24}Na , however, the upward shift was about 1.5% at ~ 4000 cts/sec, and increased monotonically to 5% at $\sim 68,000$ cts/sec.

During the experiment, the count rates in the side channels were 4000 cts/sec or less. During preliminary experiments with a copper target it was found that about 12 to 13% of the counts in the side channels were due to ^{128}I . With a duty cycle of 4% for the synchrocyclotron, the instantaneous count rate in the side channels can be as much as 88,000 cts/sec. The resulting gain shift, particularly in channel B, was taken into account by the method used to determine the variation in spectrometer efficiency.

For most spectra the number of counts observed is highest at low gamma-ray energy, and decreases with increasing energy. The average count rates in channel A were ≈ 1300 cts/sec which, with considerations similar to those for the side channels, gave instantaneous count rates of $\sim 30,000$ cts/sec. Since most of the counts are due to low-energy gamma rays, and the gain shift for those is small, no correction was believed necessary.

B. Coincidence Circuit Time Resolution and Counting Efficiency

Examination of the block diagrams for the spectrometers shows that a total of six coincidence circuits were used including those to determine the chance backgrounds for the pair spectrometer and the counting rate without time-of-flight restrictions for the anticoincidence spectrometer. For each of the "fast" circuits the time resolution was determined by the choice of clipping lines. The result was measured by delaying one signal with respect to another by means of a Helidel variable delay line. Typical values of the full width at half maximum for these time overlap or "helidel" curves for the pair spectrometer were $\tau_{AB} = 54$ nsec and $\tau_{BC} = 38$ nsec. Variations in temperature and other factors led to variations in τ of $\sim \pm 2$ nsec. τ_{BC} was reduced to less than $1/f$, where f is the extraction

frequency of the synchrocyclotron (~ 21 Mc), so that chance coincidences due to pulses produced in adjacent microbursts were effectively eliminated.

The use of resolving times as small as 36 nsec with the relatively slow amplifiers led to loss of counts in the coincidence circuits. This loss was determined by the method of Peelle²⁵ which assumes that the relative time distributions of two pulses in coincidence may be represented by normal jitter distributions. On this basis the coincidence circuit efficiency was derived in terms of the width, height, and slope at the half-height of the measured overlap curve. The loss for BC coincidences amounted to $\sim 15\%$, while for AB coincidences the loss was $\sim 1\%$.

The loss of coincidence counts does not directly affect the results obtained with the pair spectrometer since its calibration is based on the response to known sources measured with the same coincidence circuit settings. However, variations in the fraction of counts lost introduce an uncertainty in the overall efficiency of the pair spectrometer. To reduce this uncertainty in future measurements, losses in the coincidence circuit will be limited to less than 2%.

For the anticoincidence spectrometer, much longer pulses were used in the anticoincidence circuits, typical widths being ~ 65 nsec. No losses, or failures to cut off, occur with pulses this wide.

Finally, for the fast A*D coincidence circuit, the NaI(Tl) pulse was shortened to nearly the practical limit and losses due to walk and jitter are inevitable. The average loss, determined by the method described above, was $(6 \pm 2)\%$. This loss is certainly dependent on pulse height due to walk but in view of its small value, no determination of this dependence was made. This was a mistake, as demonstrated by later walk measurements made with a similar fast-timing circuit. Walks of 3-5 nsec were observed over the pulse-height range of interest. Typical resolving times for the A*D coincidence circuit were ~ 10 -12 nsec (full width at half maximum). A walk of 4 nsec from the average time position would reduce the efficiency of the fast coincidence circuit by $\sim 30\%$ and an uncertainty of this magnitude must be attached to the gamma-ray spectra. The efficacy of the

25. R. W. Peelle, Nucl. Instr. Methods 29, 293 (1964).

time-of-flight rejection of neutron-induced background is shown in a later section (III-F).

C. Chance Coincidence Backgrounds

In a multicrystal spectrometer of the type employed in this experiment, spurious counts arise due to accidental coincidences of counts in the different channels, giving rise to the so-called chance coincidence background. This section deals with the treatment of this background.

The chance coincidence background is composed of contributions from accidentally simultaneous events in all three channels, and true coincidences in two of the channels in chance coincidence with the third, that is,

$$N_{ABC}^{ch} = N_A N_B N_C (\tau_A \tau_B + \tau_B \tau_C + \tau_A \tau_C) + N_C N_{AB} (\tau_{AB} + \tau_C) \quad (1)$$

$$+ N_B N_{AC} (\tau_{AC} + \tau_B) + N_A N_{BC} (\tau_{BC} + \tau_A)$$

where N_{ABC}^{ch} is the triple chance coincidence rate, N_i is the count rate in channel i , N_{ij} is the true coincidence rate between channels i and j , and τ_{ij} is the resolving time of the coincidence circuit for events occurring in channels i and j .

To obtain the chance coincidences experimentally, another coincidence circuit identical to the one used to determine the triple coincidences was employed. The appropriate time delays for triple coincidence were established for the chance coincidence circuit also. To measure the chance coincidence components, one or more channels were set out of coincidence by the time separation between microbursts, i.e. 42 nsec, with the Helidels. A triple coincidence (pair) run was divided into four parts in order to determine the contributions from the four components of Eq. 1.

To obtain the chance coincidence background, each component was adjusted to reflect the counts which should have been observed had the measurement been made for the whole run instead of just a part, and the sum of the components taken as the total background. In order to make the background correction it was assumed that the chance spectrum is similar

in shape to the measured pair spectrum. The correction subtracted from each channel of the pair spectrum was then simply the ratio of the total chance counts to the total pair counts, multiplied by the number of counts in that channel. This correction amounted to 1.7% - 8.6%.

In the case of the total absorption spectrometer, chance events would result in a decrease in the observed count rate since the spectrometer's detectors operate in anticoincidence. Computing the chance coincidence rate in the usual fashion,

$$N_{ch} = \tau N_A N_{B+C} \quad (2)$$

where N_{ch} is the chance coincidence rate, N_A is the count rate in channel A, N_{B+C} is the sum of the count rates in channels B and C, and τ is the resolving time of the anticoincidence circuit, we found a correction amounting to less than 0.25%. Hence no correction for chance events was made for the anticoincidence data.

D. Count Losses

The use of the cross-over pickoff timing circuit (snip-snap) means that pulse pileup leads to changes in timing and thus loss of time coincidence (as may be seen by studying the combination of doubly differentiated pulse shapes). For the pair spectrometer this loss was measured by the use of a 60-cycle pulser. As indicated in the block diagram (Fig. 7), the pulser signal is injected into the cathode follower preamplifiers of two channels together with the NaI(Tl) pulse in one channel. The presence of the random signals reduces the rate observed in the coincidence output of the two channels by an amount which may be accurately measured. The loss is then related to the measured counting rate and the height of the pulser pulse. Variations with counting rate and pulse height were determined for channel B. The loss in channel C was taken equal to the loss in B with a minor correction for count rate.

Variation of the loss with pulse height across the B channel is shown in Fig. 16, together with the appropriate spectrum -- that is, the spectrum observed in B channel gated with signals from the A, B, and C channels.

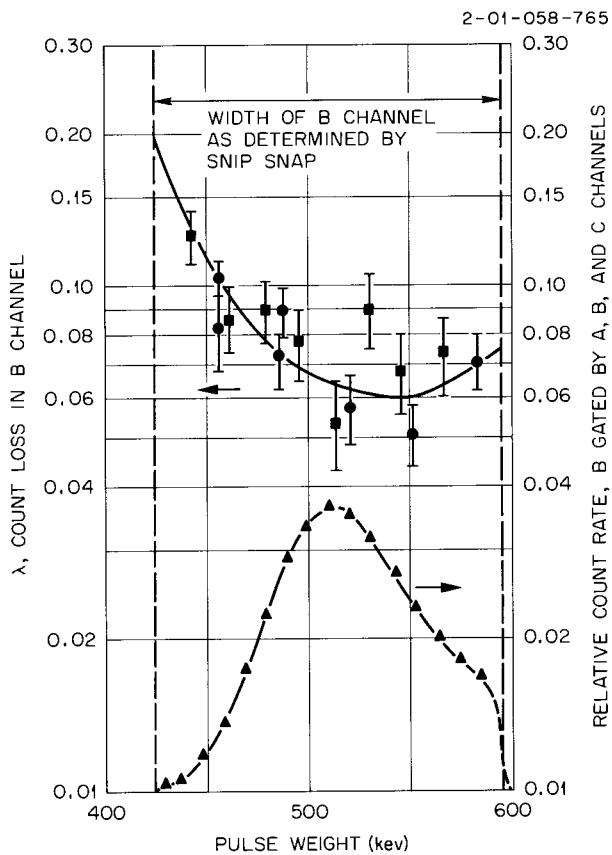


Fig. 16. Count Loss Spectrum for B Channel with 350 counts/sec in the Channel with a C Target. The lower curve is the gated B channel pulse-height spectrum.

The weighted average loss for the data shown is $\bar{\lambda} = \frac{n(\text{true}) - n(\text{observed})}{n(\text{true})}$
= 0.074 ± 0.008 . The loss at the center of the channel (511 keV) for comparison is $\lambda_{511} = 0.064 \pm 0.005$. The counting rate in the B channel was 350 cts/sec for the above determination.

It was essential that the relative count loss (λ_{511}) be measured for each target and each beam strength from the synchrocyclotron. The duty factor and thus the instantaneous counting rate varied with the setting of some of the synchrocyclotron controls. For the pair runs, the duty factor varied from 0.026 to 0.049 as determined from random coincidence measurements. These values are consistent with those reported for the Harvard Synchrocyclotron.²⁶ The effective count loss was taken equal to the measured $\lambda_{511} \times 0.074/0.064$.

The observed variation of loss with counting rate, n , was consistent with the expression for the correction factor due to the loss, $L = (1/1-\lambda)$, ($L \geq 1$):

$$L(n) = L_0(1/1 - \lambda_0)^{n-n_0/n_0} \quad (3)$$

where L_0 and λ_0 are correction factors at the initial count rate, n_0 , and

$$\lambda_0 = \frac{n_0(\text{true}) - n_0(\text{observed})}{n_0(\text{true})} .$$

The loss in the A channel was determined by the fast signal (A*) and thus the losses were negligible compared to the other channels. Losses in the D channel could arise only from using a pulse too small to fire the A*D coincidence circuit for small proton beams. The high voltage on the D photomultiplier was adjusted for each change in the proton beam strength to eliminate this possibility.

Correction factors for count losses were calculated on the basis of measured losses in Eq. 3 for each of the pair spectrometer measurements.

26. J. LeFrancois, Rev. Sci. Instr. 32, 986 (1961).

More significant than the count losses in the A channel was the distortion of the pair spectrum due to pileup. This amounted to a distortion of ~ 5 to 8% of all pulses at 1 MeV and ~ 3 to 5% at 2 MeV. These estimates are based on 60-cycle pulser measurements of the type used to determine the B losses.

For the anticoincidence spectrometer, "losses" in the side channels result in counts gained in the tail of the spectrum but not the peak. Thus this effect results in a small count-rate distortion of the tail of the response function of the spectrometer. The magnitude of the distortion was made negligible by calibrating the response at counting rates near those used in the proton experiments. Distortions in the spectrum due to pileup in the A channel amounted to less than 0.5% for the anticoincidence spectrometer, where the A rates were relatively low. Due to the high counting rates in the anticoincidence spectrometer, appreciable losses occurred in the pulse-height analyzer. These were not accurately determined and a 20 to 30% uncertainty must be attributed to this source for the low-energy gamma-ray spectra.

E. Spectrometer Efficiency

The spectrometer efficiencies were based on the measured responses to gamma-ray sources of known disintegration rate (^{198}Au , ^{137}Cs , ^{22}Na , ^{88}Y , and ^{24}Na). The disintegration rates were determined by use of a high-pressure ionization chamber which, in turn, had been calibrated by absolute coincidence counting.²⁷ Effective source strengths were determined by considering the disintegration schemes and the small attenuations within the source structure. Errors in source strength determinations ranged from 2 to 4% .

Use of the ^{88}Y and ^{24}Na sources gave values of the efficiency of the pair spectrometer at 1.368, 1.840, and 2.754 MeV, which are shown in Fig. 17. Both the total efficiencies for producing a count and the Gaussian peak efficiencies are shown. All of the efficiency values in Fig. 17 have been divided by the Hough formulation²⁸ of the Born

27. R. W. Peelle, Use of 4π High-Pressure Ionization Chambers as Secondary Standards for Calibration of Gamma-Ray Sources, ORNL-CF-61-4-32 (April 17, 1961).

28. P. V. C. Hough, Phys. Rev. 73, 266 (1948).

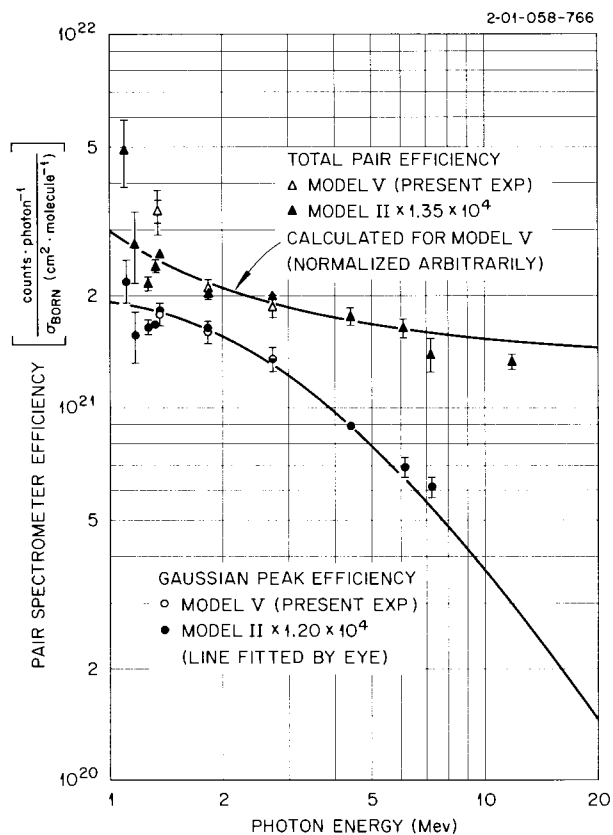


Fig. 17. Absolute Pair Spectrometer Efficiency. Results are divided by the pair cross section of NaI.

approximation to the pair cross section of NaI in order to remove the very rapid energy dependence at low gamma-ray energies. The solid angle for the spectrometer was determined by the aperture of the collimator and the size and distance away of the gamma-ray source.

It is clearly desirable that additional measurements be made with gamma-ray sources of higher energy. However, such sources are difficult to produce, and thus the energy dependence of the efficiency of the pair spectrometer used (Model V) was compared with that for another pair spectrometer (Model II) which had been calibrated to energies of ~ 12 MeV (ref. 29). As may be seen in Fig. 17, the results for the two spectrometers agree well in the region of overlap. Therefore, considerable confidence was attached to the extrapolation of the shape of the efficiency curve according to the earlier data.

In addition, the dependence of the total pair efficiency on gamma-ray energy was calculated, with results as shown in Fig. 17. For the calculation the NaI pair cross sections of West³⁰ were used. Corrections were made for attenuation in the NaI and housing (from 22 to 30%) and fast annihilation of positrons³¹ (from 1 to 18%). Annihilation radiation escape from the center crystal is independent of energy and energy loss by bremsstrahlung radiation does not affect the total efficiency. Finally, use of the NaI light piper greatly reduces the loss of positrons from the center crystal since annihilation in the light piper still gives a large solid angle for detection of the annihilation radiation in the side crystals. The positron loss varies from 0 to 5%.

Errors for the pair spectrometer efficiency varied from 5% at 1.5 to 3 Mev, to 10% at 7 MeV.

For determining the efficiency of the anticoincidence spectrometer, sources were available to cover the energy range of interest. The results, shown in Fig. 18, carry errors of $\leq 4\%$ below 2.0 MeV.

-
29. F. C. Maienschein and R. W. Peelle, Neutron Phys. Div. Ann. Progr. Rept. Sept. 1, 1960, ORNL-3016, p. 82.
 30. H. I. West, Phys. Rev. 101, 915 (1956).
 31. F. C. Maienschein and R. W. Peelle, Neutron Phys. Div. Ann. Progr. Rept. Sept. 1, 1960, ORNL-3016, p. 93.

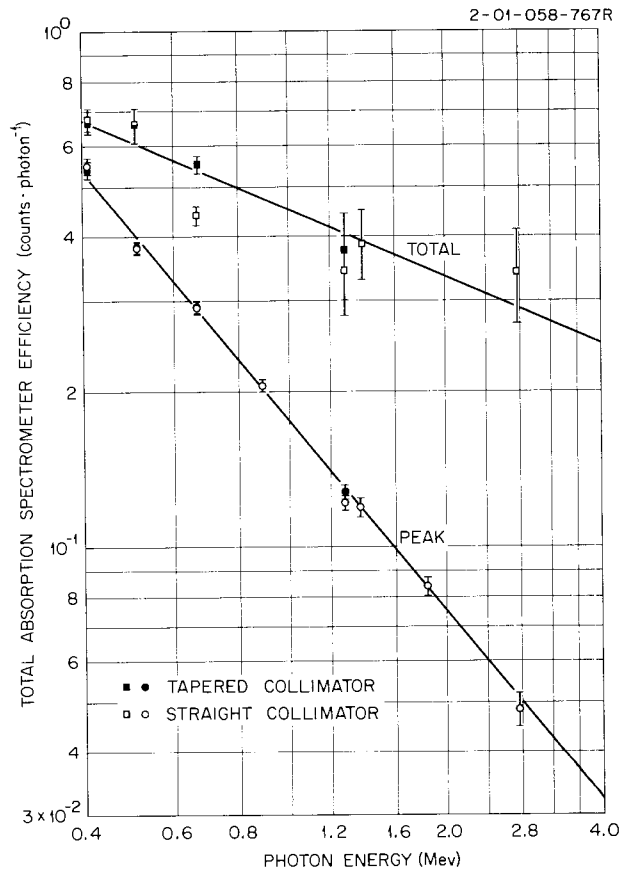


Fig. 18. Absolute Total-Absorption Spectrometer Efficiency. Consistent results are shown for two different collimators.

Exposure of the spectrometers to the known gamma-ray sources gave pulse-height spectra which were used to establish "response functions." These response functions were then used in the "unscrambling" process to be described later.

The spectrometer efficiencies varied during the experiment due to two principal causes: changes in the coincidence circuit efficiency and drifts in the side channel settings. Changes in coincidence circuit efficiency are directly reflected in the spectrometer counting rate. The effect of changes in the side channel widths on the pair-spectrometer counting rate was measured to be 0.9% per keV change in width and the stability of the snip-snaps was such that the variation from this source was unimportant. The more significant effect of count-rate-induced gain shifts in the position of the 511-keV annihilation peak was measured to be $\leq 2.8\%$ for a 1% gain change. For the anticoincidence spectrometer with its wide window on the side channel, none of these effects is significant.

Measurements with the gamma-ray sources were made of the relative efficiency of the spectrometer between all runs at the cyclotron. A ThC" source with a 2.62-MeV gamma ray and an Am-Be source, giving 4.43-MeV gamma rays from $^{12}\text{C}^*$, were used for the pair spectrometer. ^{127}Cs and ^{22}Na were used for the anticoincidence spectrometer. For the first two pair runs (carbon and aluminum targets), rather large changes in efficiency were measured (up to 19%) but thereafter the efficiency was constant within the statistical error of $\sim 7\%$. All of the relative measurements with the anticoincidence spectrometer were consistent within the errors of $\sim 4\%$.

F. Neutron Rejection Efficiency

It was pointed out above that one of the important considerations in the design of the spectrometer was the ability to reject counts caused by neutrons, either in the spectrometer or its environs. This section is concerned with evaluations of the efficacy of the design.

A first rough estimate of the fraction of neutron counts rejected can be obtained by assuming a uniform time distribution of neutron-induced counts during a macroburst, so that the fraction of rejected counts is simply the ratio of the time during which a count is rejected to the total

time of an rf cycle. These data can be obtained from delayed coincidence experiments as shown in Figs. 19, 20, and 21 for the different spectrometer positions employed. The cyclotron rf at the time of extraction corresponds to a cycle time of 42.0 ± 0.5 nsec, and the resolving time of the coincidence circuit as obtained from Figs. 19 and 20 is 11.8 ± 0.3 nsec. Under the above assumption of a neutron distribution uniform in time, the fraction of rejected neutron counts is estimated as 0.73 ± 0.02 .

It should be noted that the curve presented in Fig. 21 was not used in estimating the resolving time. It is believed that this curve is broadened by an unresolved neutron contribution. To test this hypothesis, delayed coincidence measurements were made at different distances from a thick carbon target with the spectrometer at 0° , which is the worst situation from the standpoint of neutron interference. The results are shown in Figs. 22 and 23. It is seen that broadening of the peak due to neutron contributions is already evident at 71.3 cm, with the separation becoming quite distinct at 207.6 cm. An estimate of the resolving time from these data yields 10.8 ± 0.7 nsec, which is fairly consistent with the previous result.

While the neutron rejection fraction as estimated above is useful as an approximate check on the magnitude, it is not expected to be more than qualitatively correct. The rejection fraction can be expected to be quite sensitive to the neutron spectrum, which in turn will vary with the target material and spectrometer position. To obtain a better estimate we must also have a measure of the neutron-to-gamma ratio.

An auxiliary absorption experiment was performed to measure the neutron-to-gamma ratio for one material, carbon, using the total-absorption spectrometer. The results of the experiment with lead absorbers are shown in Fig. 24. Two sets of data were taken: The number of counts in time coincidence with the microbursts as a function of absorber thickness, and the variation of total counts with absorber thickness. Extrapolating the flat portion of the curves back to zero absorber thickness yields the number of counts due to neutrons. The ratio of the number of neutron-caused counts, when subtracted from unity, is the desired neutron rejection fraction. In this case it amounts to 0.59 ± 0.01 .

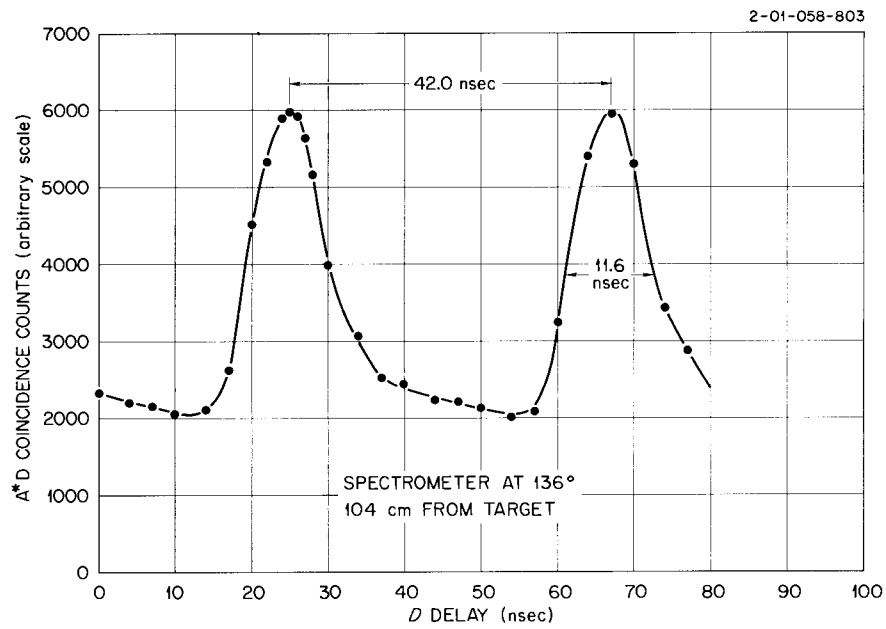


Fig. 19. Counting Rate in the A*D Fast Coincidence Circuit as a Function of Delay Introduced in the D Signal. (20-MeV-thick target at 136° and 104-cm-thick target-to-crystal separation distance.)

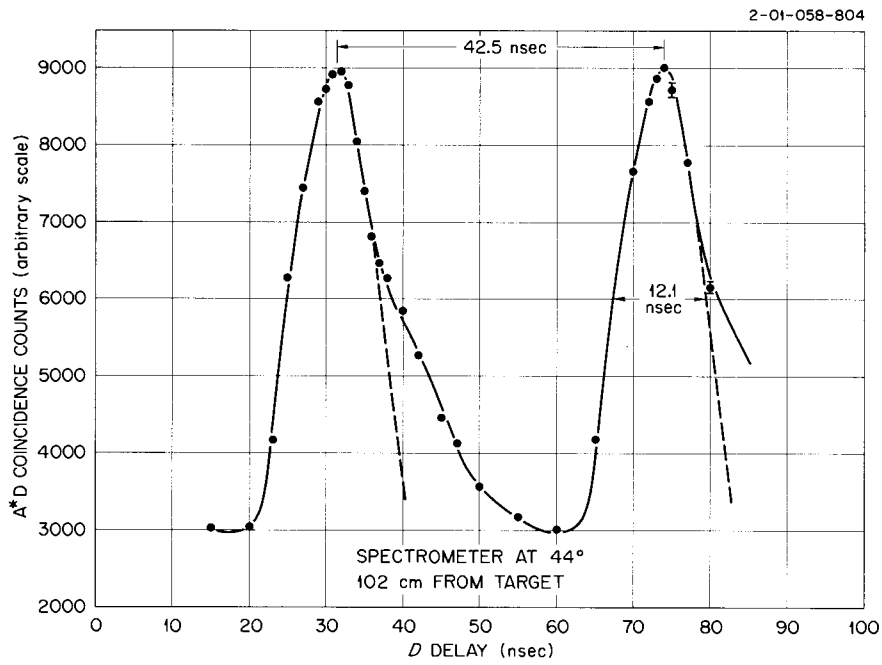


Fig. 20. Counting Rate in the A*D Fast Coincidence Circuit as a Function of Delay Introduced in the D Signal. (29-MeV-thick target at 44° and 103-cm target-to-crystal separation distance.)

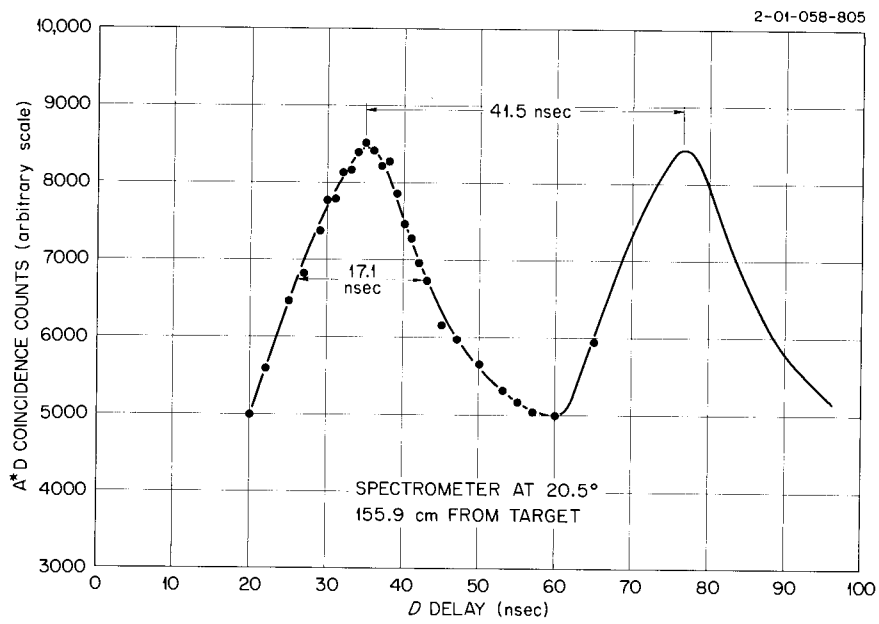


Fig. 21. Counting Rate in the A*D Fast Coincidence Circuit as a Function of Delay Introduced in the D Signal. (29-MeV-thick target at 20.5° and 156-cm target-to-crystal separation distance.)

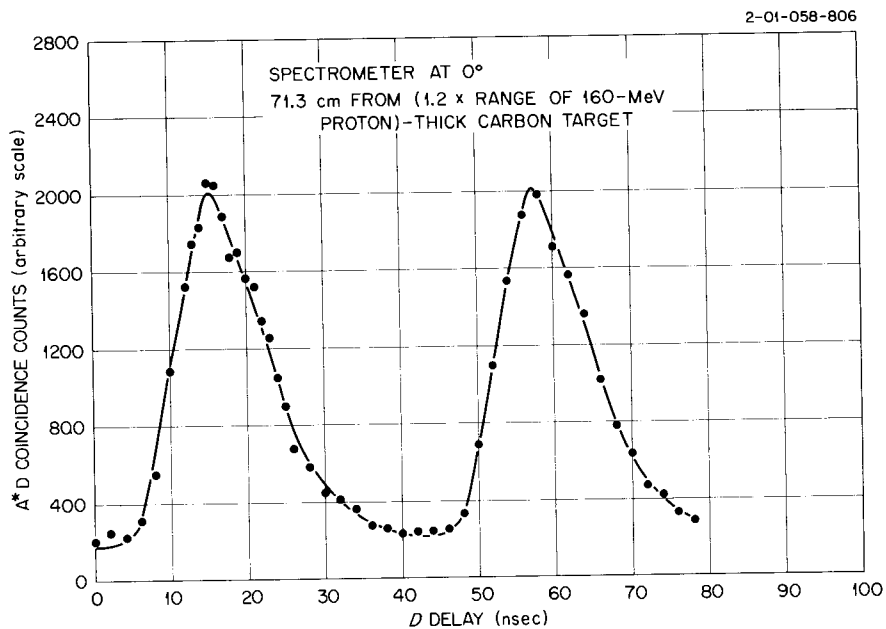


Fig. 22. Counting Rate in the A*D Fast Coincidence Circuit as a Function of Delay Introduced in the D Signal. (Target 1.2 proton ranges thick and at 0° and 71-cm target-to-crystal separation distance.)

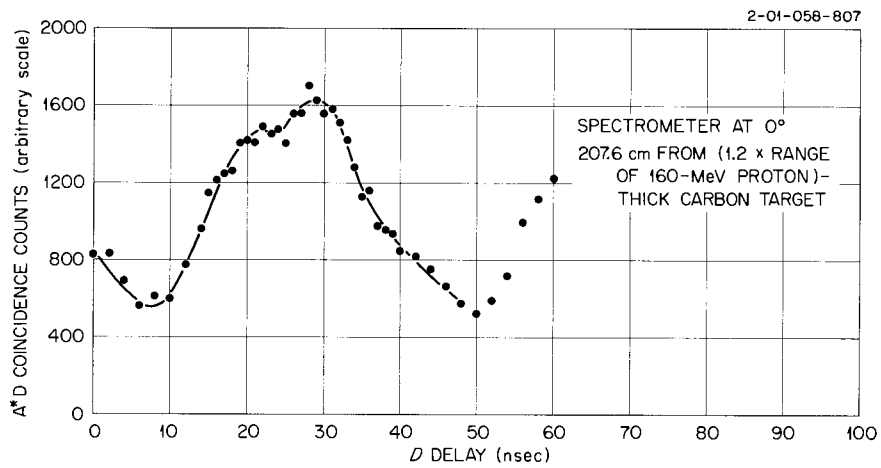


Fig. 23. Counting Rate in the A*D Fast Coincidence Circuit as a Function of Delay Introduced in the D Signal. (Target 1.2 proton ranges thick and at 0° and 208-cm target-to-crystal separation distance.)

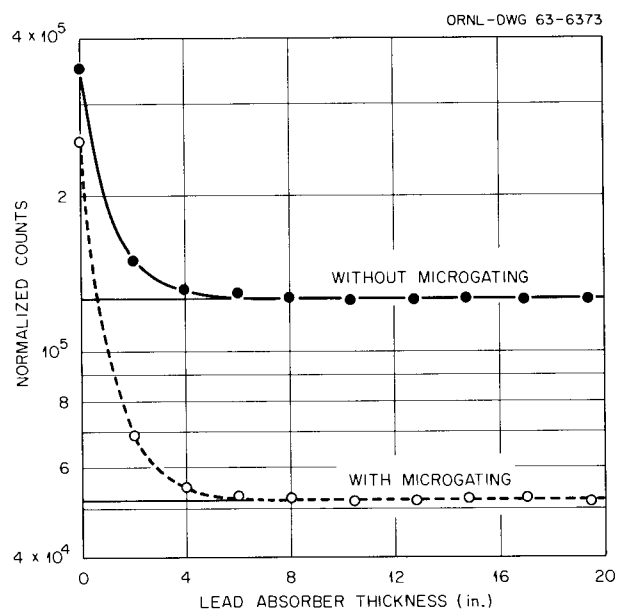


Fig. 24. Counting Rate of the Total-Absorption Spectrometer as a Function of the Thickness of Lead Absorber (29-MeV-Thick Carbon Target).

Due to time limitations it was not feasible to obtain a similar curve for each target and spectrometer position used. However, it proved feasible to measure one point on the absorption curve for each measurement with the total-absorption spectrometer. A lead absorber thickness of 12-3/4 in. was chosen as being representative. Considering the virtually zero slope of the curve, the error introduced by equating the intercept to the value measured with this absorber should be negligible. The neutron rejection fractions thus obtained are listed in Table 3. It is noteworthy that the average rejection fraction is 0.70 ± 0.01 , in good agreement with our first crude estimate.

Table 3. Neutron Rejection Fraction for Various Target Materials. Spectrometer at 136° .

Material	Neutron Rejection Fraction
Be	0.76 ± 0.01
C	0.59 ± 0.01
Al	0.68 ± 0.01
Co	0.66 ± 0.01
Bi	0.76 ± 0.01
H ₂ O	0.77 ± 0.01

It is interesting to note that the difference between the measured and extrapolated counts at zero absorber thickness as shown in Fig. 24, which should be the number of counts observed due to gamma rays, is 2.24×10^5 for the case without microgating, and 2.03×10^5 for the case with microgating. These gamma-ray figures yield a coincidence-circuit efficiency of 91%, which is in agreement with the previously determined value (see Section III-B), p 25) of $(94 \pm 2)\%$.

IV. Results and Discussion

A. Data Analysis

The output of the spectrometer discussed in Section II is, of course, a pulse-height spectrum; the desired information, however, is the

corresponding photon spectrum. It is necessary, therefore, to "unscramble" the pulse-height spectrum to obtain the spectrum of the incident photons.

The unscrambling method used on our data is that of Burrus.⁸ It uses the known non-negativity of the incident gamma-ray spectrum as an additional condition in establishing an approximation to a spectrum which would be observed with an ideal spectrometer having a pure Gaussian response function to a monoenergetic gamma ray. Two results are computed, one everywhere greater, and the other everywhere less, than the "true" spectrum. The method considers the errors assigned to the input data and the response matrix, and utilizes this information to yield, between these two limits, a confidence interval such that a specified fraction of an ensemble of experiments would fall within these limits. In our case the 68% confidence interval was chosen.

The data were divided by the fractional solid angle subtended by the detector, the number of incident protons, and the target thickness. The effects of chance coincidences in the pair spectrometer runs were subtracted by measuring the total number of chance coincidences and assuming that their distribution was similar to that of the foreground spectrum. Neutron contributions to the total absorption spectrometer runs were measured by closing the collimator with 12-3/4 in. of lead (see Section IV-F), and subtracting the resulting spectrum from the one obtained with the open collimator. Corrections ($\leq 1.19 \pm 0.09$) for variations in the spectrometer efficiency were also applied to the data.

A constant correction of 0.94 ± 0.02 for the efficiency of the fast coincidence circuit was made. It later developed that this correction varies rather strongly with energy due to the walk of the fast signal in the A channel. Since the exact energy dependence was not measured, the correction is not made in the spectra presented. However, an additional uncertainty of 30% is included in the error attached to the cross sections. Also not shown in the spectra is a correction for the absorption of the gamma rays in the target itself; however, this correction was applied to the cross sections calculated from the data. A correction for the count losses existing in the pair mode of the spectrometer, varying from 1.46 ± 0.20 to 2.14 ± 0.73 , is included in the spectra

presented. An analogous correction for the data taken in the total absorption mode amounted to $< (3 \pm 1.5)\%$. Counts lost in the side channels would result in a gain of anticoincidence counts, but the spectrum of these counts is distorted to lower energies with respect to the true spectrum. Counts lost in the center channel do not introduce such spectrum shift. The governing loss, however, is not in the electronics of the center channel but in the multichannel analyzer. It was difficult to obtain an accurate correction for this loss and only an approximate correction (1.0 ± 0.2) was included in the cross section calculations.

B. Spectra and Cross Sections at 136°

Data taken at 136° to the direction of the incident proton beam, with a separation distance of (104.1 ± 0.2) cm between the center of the "A" crystal and the target center, are presented in Figs. 25-30. It must be noted that the unscrambling program only gives the bounds of the 68% confidence interval; hence, only this confidence band is shown.

1. Beryllium (Fig. 25). Two prominent gamma rays appear in the spectrum, at (987 ± 10) keV and at (3575 ± 15) keV. The apparent line at 475 keV is probably affected by the bias of the spectrometer, hence is not considered reliable. Additional, and quite weak, lines are indicated as shown in Table 4.

The 987-keV gamma ray is assigned to the transition from the 978-keV state in ${}^8_3\text{Li}$, to the ground state [${}^9_4\text{Be}(p,2p){}^8_3\text{Li}$]; the 3575-keV line is assigned to the ground state transition from the second excited state (3560 keV) in ${}^6_3\text{Li}$ [${}^9_4\text{Be}(p,\alpha){}^6_3\text{Li}$]. Plausible assignments of reactions responsible for the weak gamma rays are also shown in Table 4.

The cross section for production of the 987-keV gamma ray by 160-MeV protons incident on a beryllium target is (1.69 ± 0.14) mb; that for the production of the 3575-keV gamma ray is (2.02 ± 0.68) mb. This value compares quite well with the (2.4 ± 0.4) mb quoted by Clegg *et al.*³² Cross sections for the weak gamma rays are listed in Table 4.

32. A. B. Clegg *et al.*, *op. cit.*

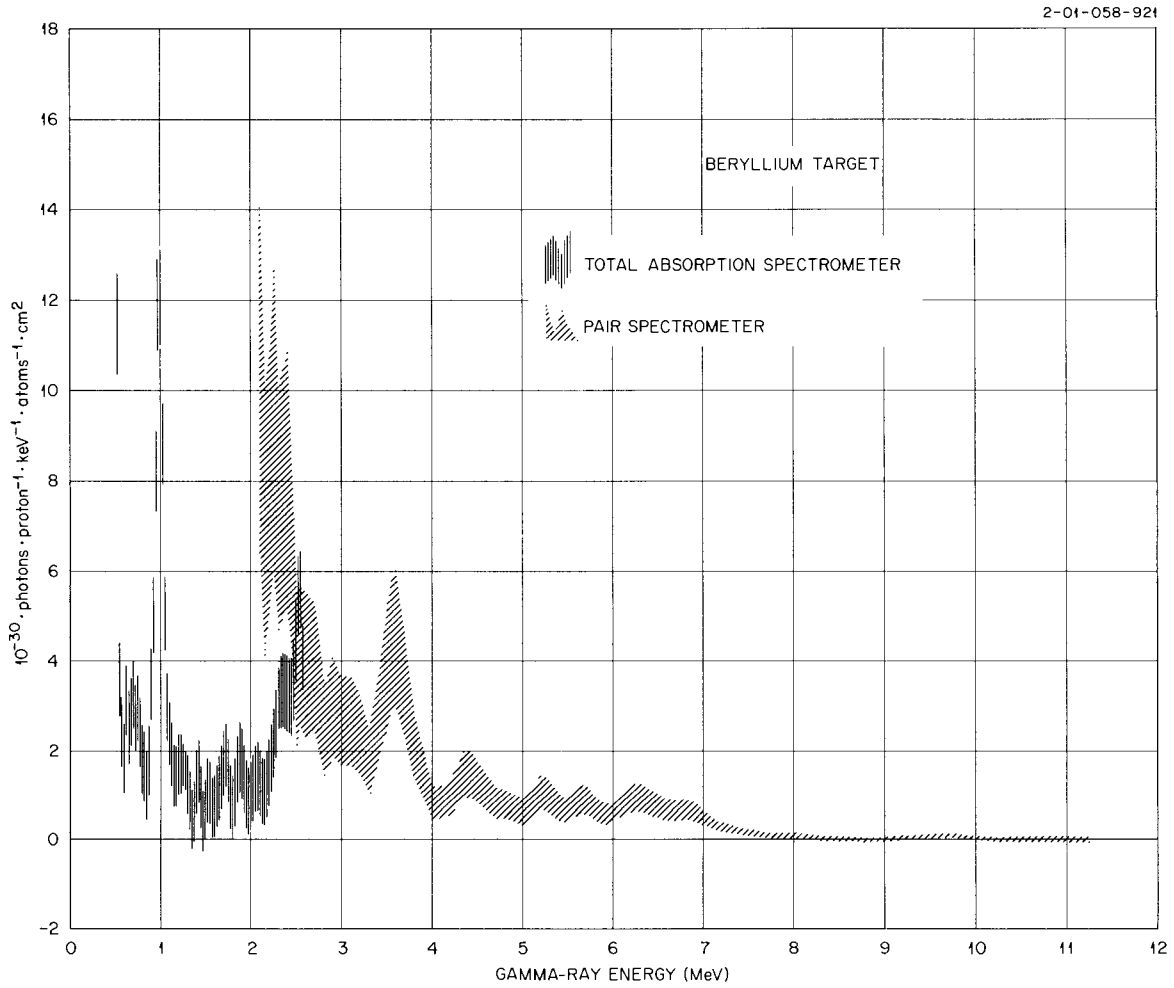


Fig. 25. Absolute Gamma-Ray Yield as a Function of Gamma-Ray Energy Due to the Bombardment by 160-MeV Protons of a 29-MeV-Thick Beryllium Target.

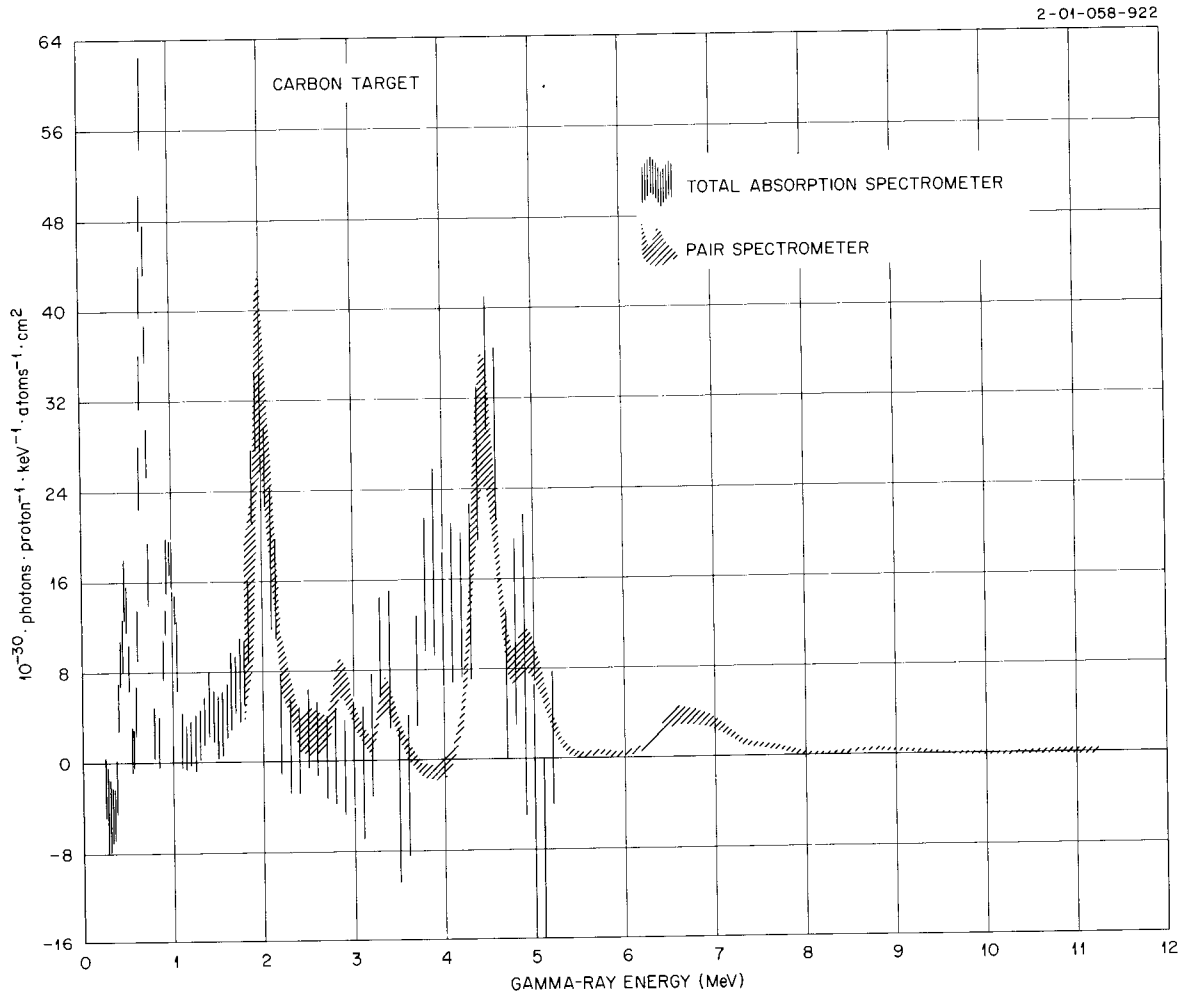


Fig. 26. Absolute Gamma-Ray Yield as a Function of Gamma-Ray Energy Due to the Bombardment by 160-MeV Protons of a 29-MeV-Thick Carbon Target.

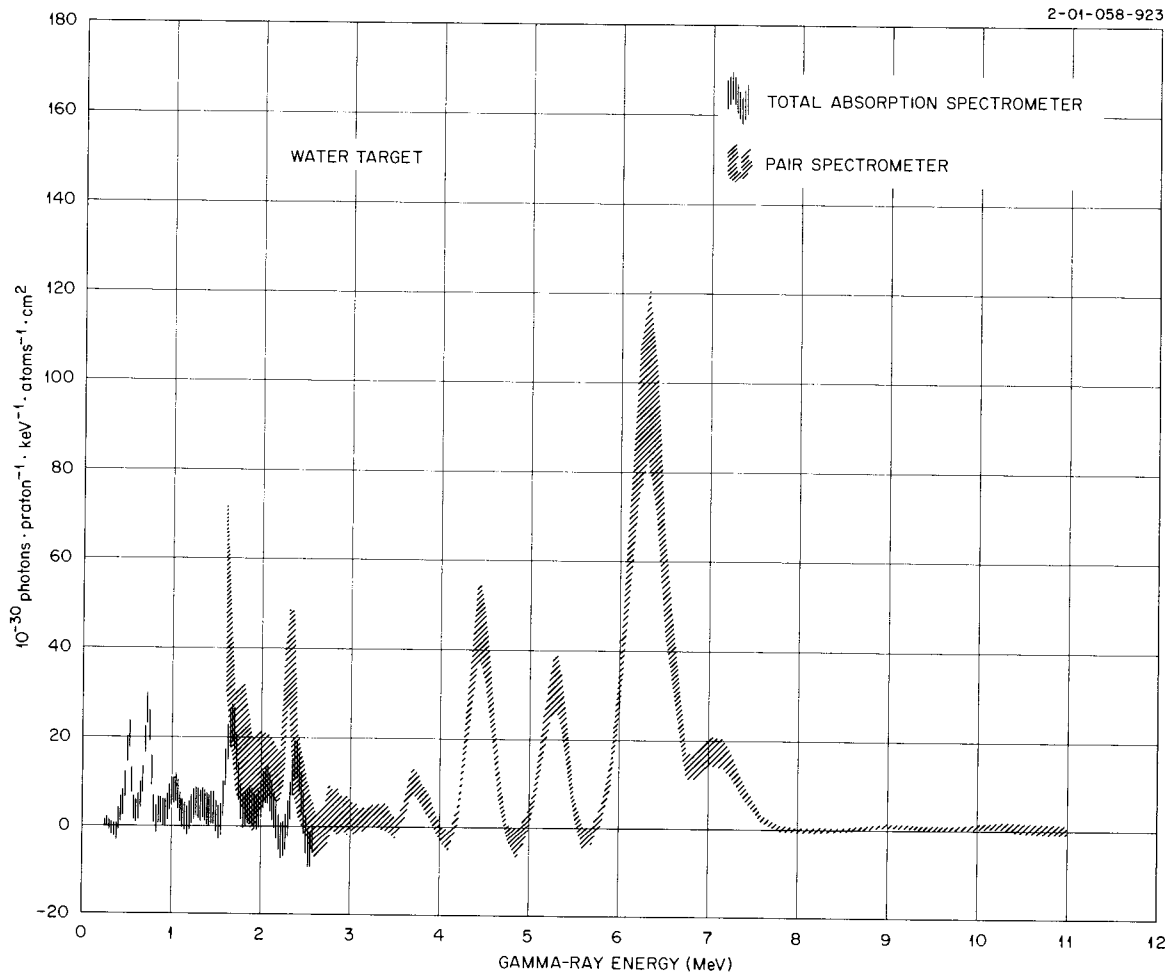


Fig. 27. Absolute Gamma-Ray Yield as a Function of Gamma-Ray Energy Due to the Bombardment by 160-MeV Protons of a 29-MeV-Thick Water Target.

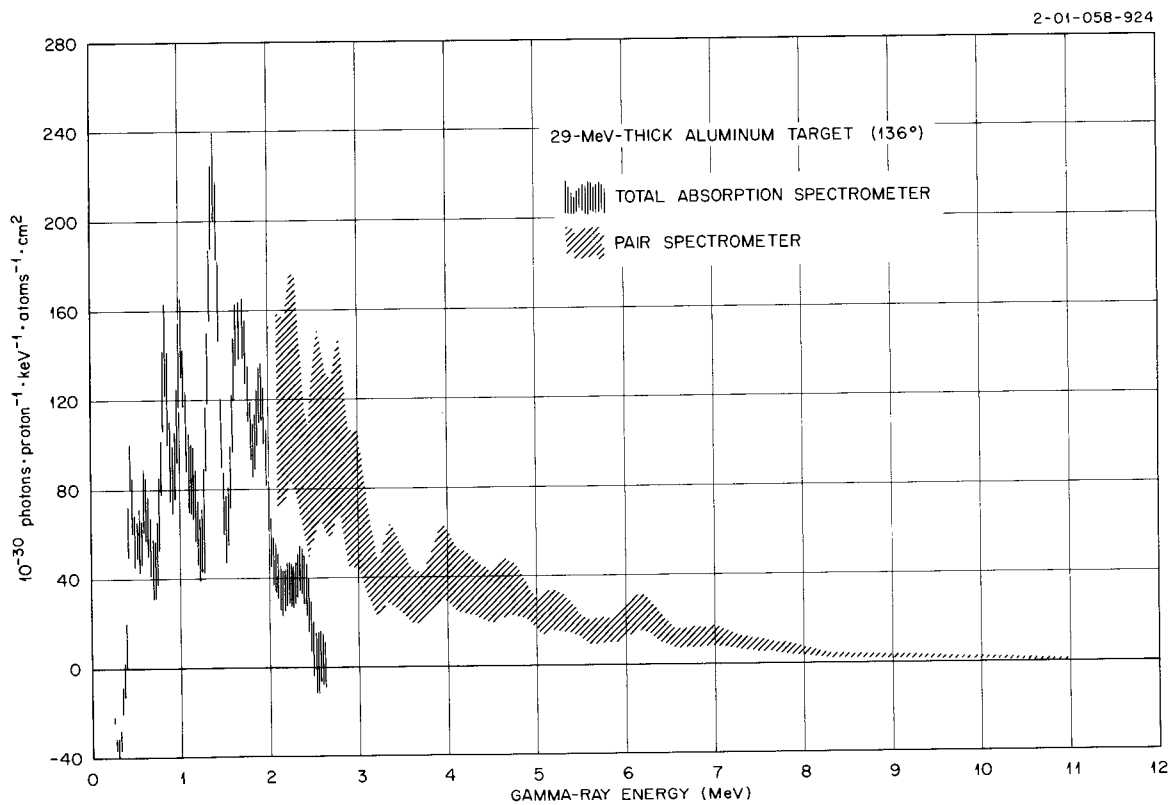


Fig. 28. Absolute Gamma-Ray Yield as a Function of Gamma-Ray Energy Due to the Bombardment by 160-MeV Protons of a 29-MeV-Thick Aluminum Target.

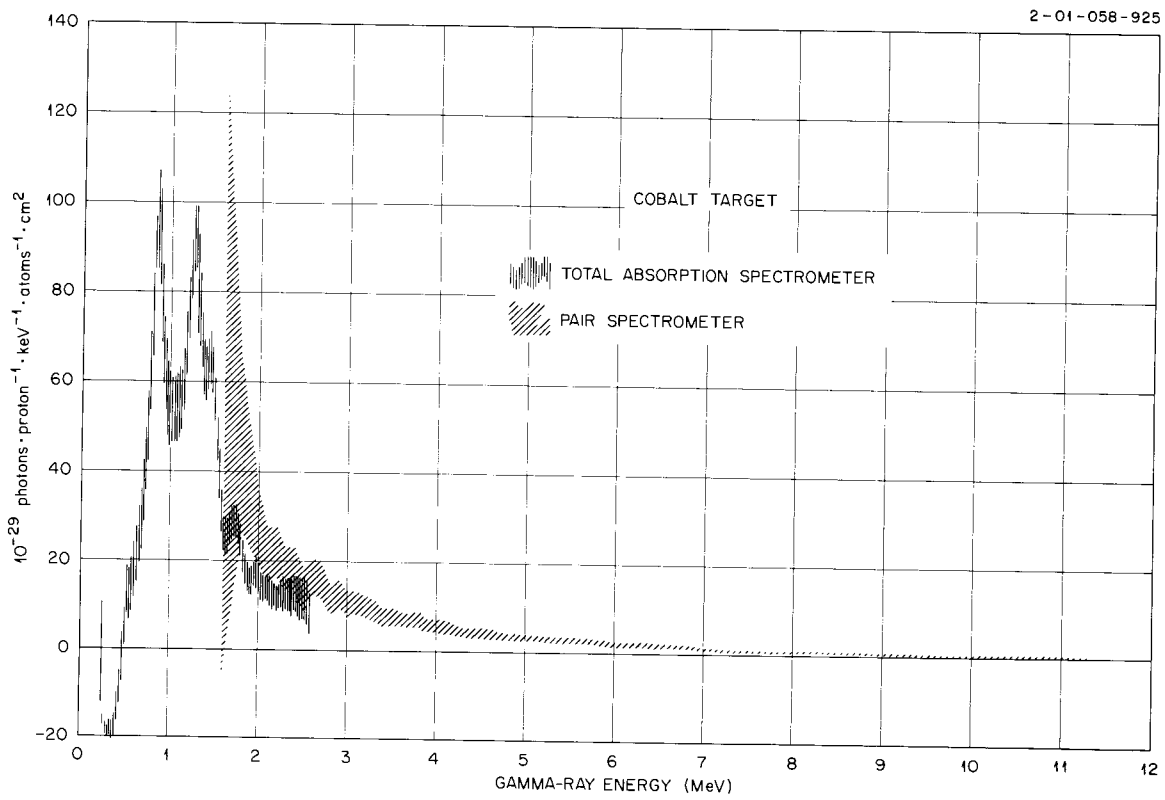


Fig. 29. Absolute Gamma-Ray Yield as a Function of Gamma-Ray Energy Due to the Bombardment by 160-MeV Protons of a 12-MeV-Thick Cobalt Target.

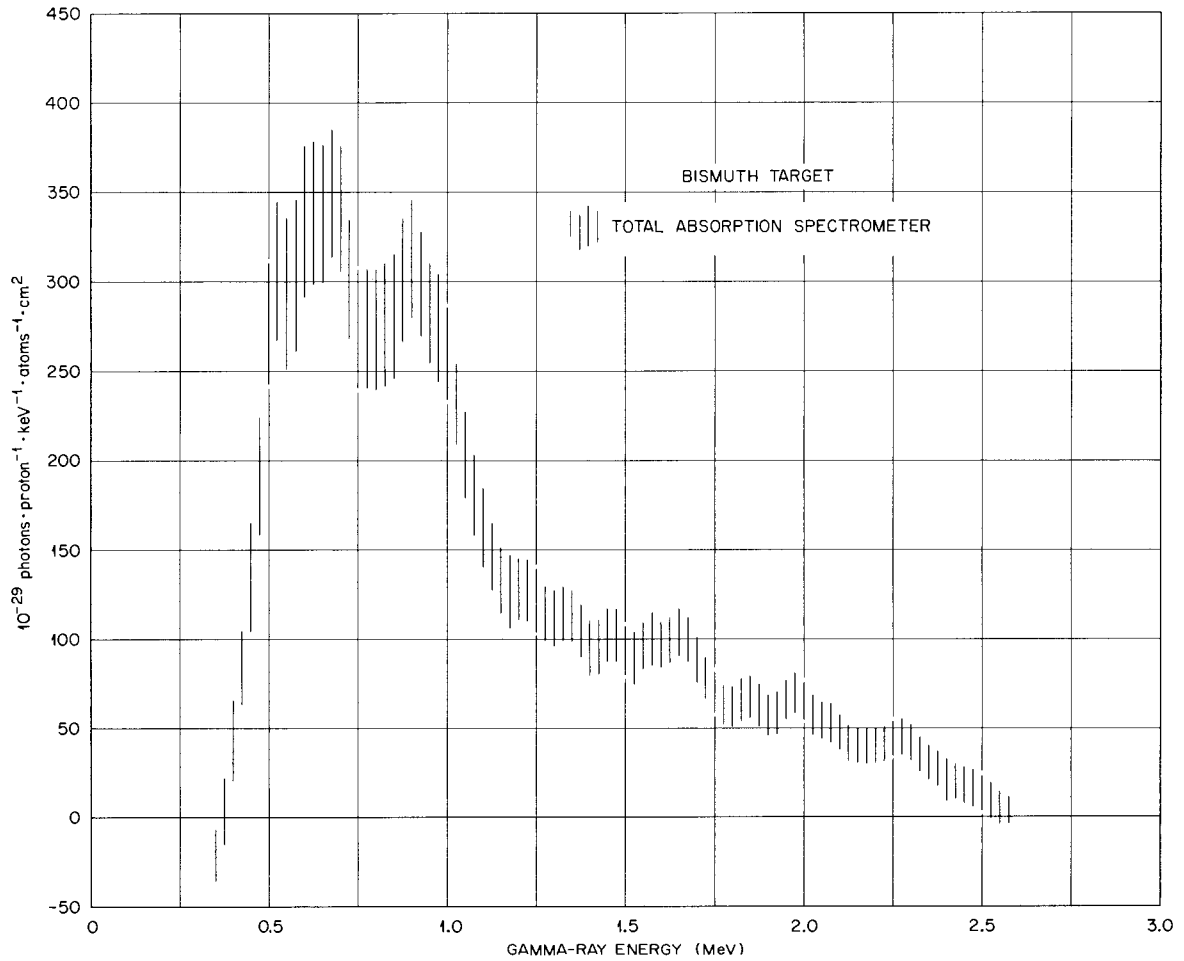


Fig. 30. Absolute Gamma-Ray Yield as a Function of Gamma-Ray Energy Due to the Bombardment by 160-MeV Protons of a 12-MeV-Thick Bismuth Target.

Table 4. Measured Energies and Cross Sections of Gamma Rays from a Beryllium Target Bombarded by ~ 160-MeV Protons

E_γ (MeV) Measured	σ (mb) Measured	Spectrometer ^a	Possible Transition	
			Reaction	Energy
987 \pm 10	1.69 \pm 0.63	T	${}^9_4\text{Be}(p, 2p){}^8_3\text{Li}$	987
1447 \pm 10	0.18 \pm 0.10	T		
1536 \pm 10	0.15 \pm 0.10	T		
1718 \pm 15	0.28 \pm 0.14	T	${}^9_4\text{Be}(p, 3pn){}^6_2\text{He}$	1710
1878 \pm 15	0.27 \pm 0.15	T		
2069 \pm 15	0.24 \pm 0.13	T	${}^9_4\text{Be}(p, \alpha){}^6_3\text{Li}$	2184
3575 \pm 15	2.02 \pm 0.91	P	${}^9_4\text{Be}(p, \alpha){}^6_3\text{Li}$	3560
4390 \pm 38	0.72 \pm 0.34	P		
5225 \pm 30	0.40 \pm 0.20	P	${}^9_4\text{Be}(p, \alpha){}^6_3\text{Li}$	5350
5675 \pm 25	0.42 \pm 0.25	P		
6250 \pm 35	0.46 \pm 0.22	P	${}^9_4\text{Be}(p, \alpha){}^6_3\text{Li}^*$	6190

*Denotes transition between excited states.

a. T = total absorption configuration; P = pair configuration.

A calculation by Bertini³³ of the nonelastic cross section for 160-MeV protons incident on beryllium yields a value of (196 \pm 2) mb. The error quoted for this and subsequent calculated values is based solely on the statistics of the Monte Carlo calculations. Summing our partial cross sections for the production of gamma rays with energies greater than 600 keV gives (6.8 \pm 1.3) mb.

2. Carbon (Fig. 26). The carbon spectrum contains quite a number of distinct gamma rays. As in the case of beryllium, and in fact in all cases in this experiment, gamma rays with energy below ~ 500 keV are not considered since the bias of the spectrometer is apt to affect them.

33. H. W. Bertini, private communication.

In this particular case a large overlap region exists between data from the spectrometer in the pair mode and in the total absorption mode. The uncertainty in the calibration of the total absorption spectrometer above 2.75 MeV is reflected in the rather large error in the data taken with that spectrometer above ~ 3 MeV.

The agreement of the data taken in the two modes is quite good, except for the absence of the 2874-keV line in the total absorption data. No good reason can be adduced for this absence, except for the fact that the spectrometer should not be used in this mode for energies above ~ 2.5 MeV; the peak may then have been lost in the uncertainty of the data during the "unscrambling."

Table 5 shows the gamma rays observed from a carbon target bombarded by 160-MeV protons, the partial cross sections for production of these gamma rays, and assignments of possible transitions for them. For comparison, the values of Clegg *et al.*³² are also shown.

It appears that our cross section values tend to be somewhat higher than those of the Oxford group, particularly at the lower energies where the total absorption spectrometer was used reliably.

If we again add the partial cross sections for production of gamma rays with energies greater than 600 keV, we get (41.4 ± 6.3) mb; Bertini's calculations³³ result in a computed nonelastic cross section of (233 ± 4) mb.

3. Oxygen (Fig. 27). The spectrum from oxygen, like the spectrum from carbon, shows a number of discrete gamma rays. Most of the activity is due to gamma rays with energy above 4 MeV; in the other cases which we investigated, the intensity generally decreased with increasing energy.

Comparison with the work of Foley *et al.*³⁴ shows generally good agreement with the data obtained using the total absorption spectrometer,

34. K. J. Foley *et al.*, Nucl. Phys. 31, 43 (1962).

Table 5. Measured Energies and Cross Sections of Gamma Rays from a Carbon Target Bombarded by ~ 160-MeV Protons

E_γ (keV) Measured	σ (mb) Measured	Spectrometer	Oxford Group	Possible Transition	
				Reaction	Energy
695 ± 17	7.13 ± 2.60	T	$4.5 \pm .5$	$^{12}_6\text{C}(p, 2pn)^{10}_5\text{B}$	717
980 ± 18	3.55 ± 1.33	T	$1.8 \pm .2$	$^{12}_6\text{C}(p, 4pn)^8_3\text{Li}$	980
1982 ± 27	8.51 ± 3.12	T	$3.9 \pm .4$	$^{12}_6\text{C}(p, pn)^{11}_6\text{C}$	1990
2014 ± 40	5.44 ± 1.99	P			
2872 ± 35	1.72 ± 0.63	P	$0.9 \pm .4$	$^{12}_6\text{C}(p, 2pn)^{10}_5\text{B}^*$	2870
3335 ± 36	2.00 ± 1.37	T		$^{12}_6\text{C}(p, 3p)^{10}_4\text{Be}$	3368
3370 ± 30	1.64 ± 0.61	P			
4480 ± 50	10.9 ± 4.1	T	6.6 ± 1.0	$^{12}_6\text{C}(p, p')^{12}_6\text{C}$	4433
4470 ± 15	11.4 ± 4.1	P			
4930 ± 35	4.08 ± 1.46	P	2.3 ± 1.0	$^{12}_6\text{C}(p, 2p)^{11}_5\text{B}$	5030
6750^a	3.03 ± 1.09	P	$2.1 \pm .7$		
8795 ± 50	0.37 ± 0.15	P		$^{12}_6\text{C}(p, 2p)^{11}_5\text{B}$	8920

a. Average energy for several gamma rays, not resolved.

*Denotes transition between excited states.

and a discrepancy by about a factor of two or three with the results from the pair spectrometer, our data being higher. It would be easy to assign this difference to an inherent systematic difference between the spectrometer used by Foley *et al.* and by us, were it not for the fact that in a carbon target an opposite difference was observed, i.e., the data from the total absorption spectrometer gave larger cross sections than observed by the Oxford group while the results from the pair spectrometer generally agreed.

Table 6 shows the gamma rays observed from a water target, the partial cross sections for their production and plausible transitions which would yield these gamma rays. For comparison, the results of Foley et al. are also included.

Table 6. Measured Energies and Cross Sections of Gamma Rays from a Water Target Bombarded by ~ 160-MeV Protons

E_γ (keV) Measured	σ (mb) Measured	Spectrometer	Oxford Group	Possible Transition	
				Reaction	Energy
727 ± 10	3.25 ± 1.24	T	3.9 ± 1.0	$^{16}_8\text{O}(p, \alpha 2pn)^{13}_5\text{B}$	717
1668 ± 10	4.4 ± 1.8	T	1.7 ± 0.5	$^{16}_8\text{O}(p, 2pn)^{14}_7\text{N}^*$	1634
2060 ± 10	1.7 ± 1.3	T		$^{16}_8\text{O}(p, 2p)^{15}_7\text{N}^*$	2034
2392 ± 10	2.5 ± 1.4	T			
2320 ± 25	6.7 ± 3.0	P	2.9 ± 0.8	$^{16}_8\text{O}(p, 2pn)^{14}_7\text{N}$	2311
3720 ± 30	2.8 ± 1.3	P		$^{16}_8\text{O}(p, 3pn)^{13}_6\text{C}$	3680
4430 ± 30	15.8 ± 5.7	P	8.3 ± 1.7	$^{16}_8\text{O}(p, p\alpha)^{12}_6\text{C}$	4433
				$^{16}_8\text{O}(p, pn)^{15}_8\text{O}$	5240
5260 ± 25	12.0 ± 4.9	P	2.6 ± 0.7	$^{16}_8\text{O}(p, 2p)^{15}_7\text{N}$	5276
6290 ± 35	55.6 ± 19.7	P	22.7 ± 3.0	$^{16}_8\text{O}(p, 2p)^{15}_7\text{N}$	6328
7100 ± 50	12.3 ± 4.4	P	2.8 ± 0.7	$^{16}_8\text{O}(p, p')^{16}_8\text{O}$	7120

*Denotes transition between excited states.

The sum of the experimental partial cross sections for the production of gamma rays with energies in excess of 600 keV is (114.6 ± 21.9) mb. The nonelastic cross section calculated by Bertini is (296 ± 3) mb.

4. Aluminum (Fig. 28). For this run, the thinner of the targets listed in Table 1 (6.808 g/cm^2) was used.

Aluminum is the lowest Z material in which we observed, in addition to discrete lines, a continuum. This continuum is probably due to many gamma rays from de-excitation of closely spaced, highly excited states which were not resolved by our equipment.

Table 7 lists the observed gamma rays, partial cross sections for their production, and some possible transitions which may give rise to the observed gamma rays. In choosing the possible transitions we considered

Table 7. Measured Energies and Cross Sections of Gamma Rays from an Aluminum Target Bombarded by ~ 160-MeV Protons

E_γ (keV) Measured	σ (mb) Measured	Spectrometer	Oxford Group	Possible Transition	
				Reaction	Energy
845 ± 10	12.4 ± 5.3	T	11 ± 2	${}^{27}_{13}\text{Al}(p, pn){}^{26}_{13}\text{Al}^*$	830
1026 ± 10	14.0 ± 7.7	T	14 ± 3	${}^{27}_{13}\text{Al}(p, pn){}^{26}_{13}\text{Al}^*$	1010
1392 ± 10	30.4 ± 11.4	T	31 ± 4	${}^{27}_{13}\text{Al}(p, \alpha){}^{13}_{12}\text{Mg}$	1369
1677 ± 10	21.9 ± 8.8	T	18 ± 3.5	${}^{27}_{13}\text{Al}(p, pn){}^{26}_{13}\text{Al}^*$	1640
1877 ± 10	13.2 ± 6.4	T		${}^{27}_{13}\text{Al}(p, pn){}^{26}_{13}\text{Al}$	1850 1880*
2250 ± 25	7.3 ± 9.2	P	7.1 ± 1.7	${}^{27}_{13}\text{Al}(p, p'){}^{27}_{13}\text{Al}$	2219
2560 ± 35	7.3 ± 7.7	P	8.8 ± 2.2	${}^{27}_{13}\text{Al}(p, pn){}^{26}_{13}\text{Al}$	2540
2770 ± 50	10.7 ± 8.4	P		${}^{27}_{13}\text{Al}(p, \alpha){}^{24}_{12}\text{Mg}^*$	2753
3400 ± 20	2.2 ± 5.1	P		${}^{27}_{13}\text{Al}(p, 2pn){}^{25}_{12}\text{Mg}$	3410
3975 ± 25	6.4 ± 6.2	P		${}^{27}_{13}\text{Al}(p, 2pn){}^{25}_{12}\text{Mg}^*$	3920
4630 ± 35	7.0 ± 6.2	P		${}^{27}_{13}\text{Al}(p, pn){}^{26}_{13}\text{Al}^*$	4600 4620
5165 ± 50	3.1 ± 4.1	P		${}^{27}_{13}\text{Al}(p, pn){}^{26}_{13}\text{Al}^*$	5120 5140
6140 ± 50	5.8 ± 4.5	P		${}^{27}_{13}\text{Al}(p, pn){}^{26}_{13}\text{Al}^*$	6190

*Denotes transition between excited states.

simplicity of the proton reaction, giving preference to those in which the smallest number of particles were emitted. In assigning the transitions, the relative prominence of the observed lines was also taken into account; thus, transitions between excited states were expected to lead to states from which ground state transitions, or cascades to the ground state, were also observed. This criterion was qualified by accepting cascades in which one member fell below the instrumental threshold (~ 600 keV).

Again data reported by Foley et al. are included in the table for comparison.

Summing these partial cross sections for gamma-ray production yields (142 ± 26) mb, while Bertini's calculations give (427 ± 4) mb. It should be noted that the experimental number does not include the continuum, which amounts to (292 ± 93) mb. The total cross section for production of photons with energies greater than 600 keV is then (434 ± 97) mb.

5. Cobalt (Fig. 29). It is apparent from Fig 29 that, except for the low energies, there is essentially no structure in the cobalt spectrum. Over most of the energy region the continuum dominates.

Four gamma rays are distinguishable at the lower energies: at 857 keV, at 1264 keV, at 1452 keV, and at 1745 keV. The latter three gamma rays are believed due to inelastic scattering. The first line is assigned to the ${}^{59}_{27}\text{Co}(p,n){}^{59}_{28}\text{Ni}$ reaction to the 0.87-MeV state.

The results are summarized in Table 8.

The sum of the partial cross sections for these discrete gamma rays is (436 ± 96) mb; the result of Bertini's calculations is (732 ± 5) mb. The continuum above 600 MeV would add (611 ± 203) mb for a total of (1.05 ± 0.22) b. This implies emission of more than one gamma ray per non-elastic event.

6. Bismuth (Fig. 30). Only the total absorption spectrometer was used with the bismuth target due to time limitations. It is reasonable to expect, however,

Table 8. Measured Energies and Cross Sections of Gamma Rays from a Cobalt Target Bombarded by ~ 160-MeV Protons

E_γ (keV) Measured	σ (mb) Measured	Spectrometer	Possible Transition	
			Reaction	Energy
857 ± 12	153 ± 60	T	$^{59}_{27}\text{Co}(p,n)^{59}_{28}\text{Ni}$	870
1264 ± 10	169 ± 65	T	$^{59}_{27}\text{Co}(p,p')^{59}_{27}\text{Co}$	1289
1452 ± 15	86 ± 33	T	$^{59}_{27}\text{Co}(p,p')^{59}_{27}\text{Co}$	1479
1745 ± 20	28 ± 15	T	$^{59}_{27}\text{Co}(p,p')^{59}_{27}\text{Co}$	1743

that no structure would have been observed at higher energies. The possible number of final states resulting from the bombardment of bismuth with 160-MeV protons can be expected to be even greater than for cobalt, where essentially no structure was observed. Even at low energies, where we observed some discrete lines in cobalt, it seems inadvisable to try to extract discrete lines from the bismuth data.

Table 9 is included to summarize the comparison between the measured cross sections for the production of gamma rays above 600 keV and the calculated total nonelastic cross sections. As would be expected, gamma-ray emission is less likely for the lighter nuclei.

Table 9. Measured Cross Sections for the Production of Gamma Rays Having Energies Above 600 keV Compared to Calculated Total Nonelastic Cross Sections

Material	Measured Cross Section (mb)	Calculated Cross Section (mb)
Be	6.8 ± 1.3	196 ± 2
C	41.4 ± 6.3	233 ± 4
O	115 ± 22	296 ± 3
Al	434 ± 97	427 ± 4
Co	1050 ± 220	732 ± 5

C. Spectra at Other Angles

In addition to the data discussed above, we also made measurements, with aluminum targets only, at 44° to the incident beam with a separation distance of (102.8 ± 0.2) cm, and at 20.5° with a (155.9 ± 0.2) cm separation.

At both these locations the total-absorption spectrometer only was used to gather data from the same target we used at 136° , i.e., 6.808 g/cm². This restriction was due to time limitations. The spectra so obtained are shown in Fig. 31, together with the pertinent spectrum from 136° . It is seen that there is essentially no difference in the three spectra, indicating isotropic emission of the prominent gamma rays.

Another set of measurements, using both the total-absorption spectrometer and the pair spectrometer at 44° , utilized a thick (26.71 g/cm², approximately 20% greater than the range of 160-MeV protons) aluminum target. The primary purpose of the measurements was to provide an experimental result for comparison with transport calculations. These spectra are shown in Fig. 32.

D. Further Studies

Clearly the hazard posed to manned space flight due to secondary gamma radiation cannot be assessed on the basis of these data alone. Additional measurements are needed, especially at lower proton energies. Planning for such measurements is at an advanced stage. When information is experimentally available on the dependence of gamma-ray production upon proton energy, it will be necessary to use these "source data" in gamma-ray attenuation calculations in order to determine the biological effect behind a shield.

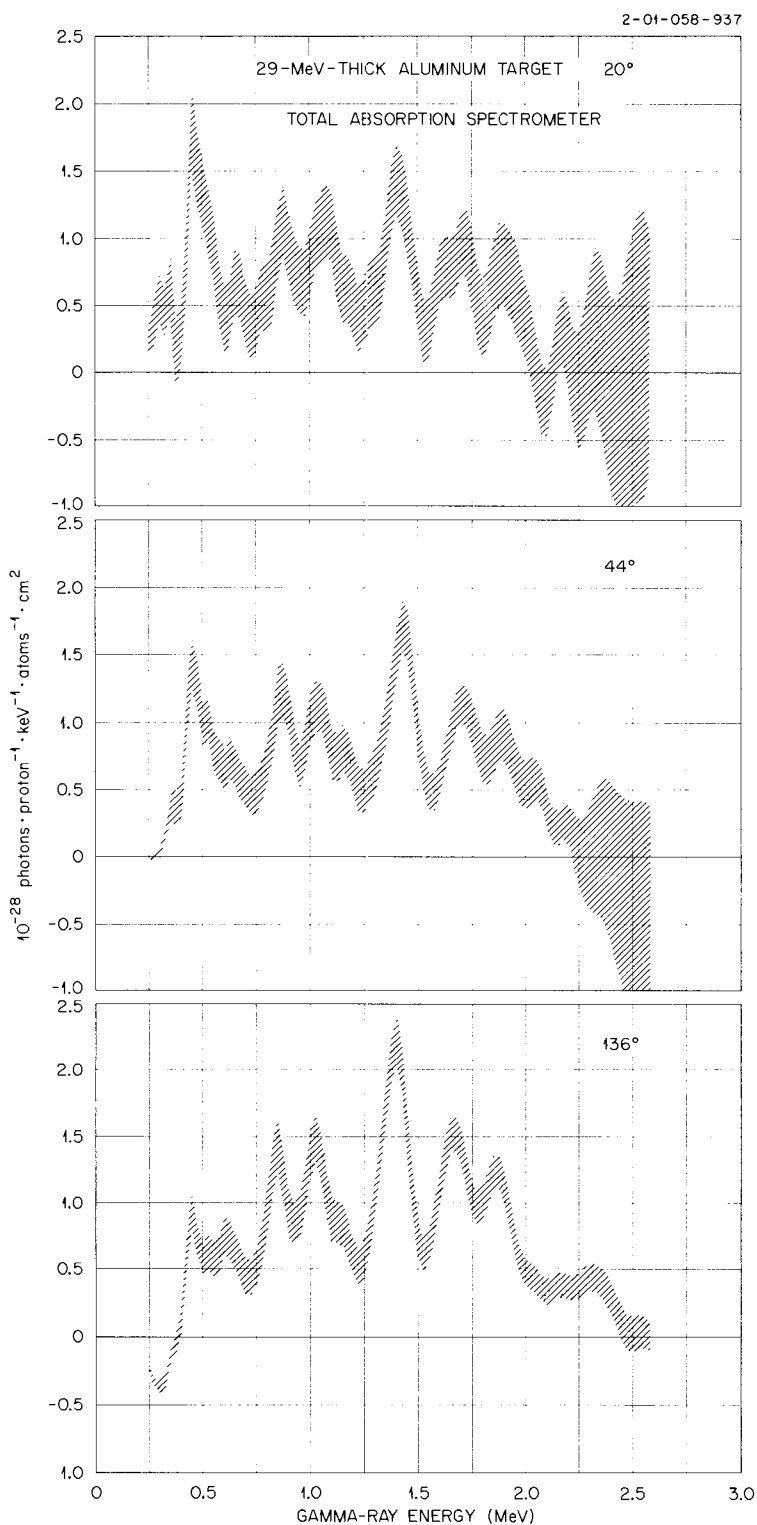


Fig. 31. Absolute Gamma-Ray Yield as a Function of Gamma-Ray Energy Due to the Bombardment by 160-MeV Protons at a 29-MeV-Thick Aluminum Target at Angles of (a) 20.5°, (b) 44°, and (c) 136°.

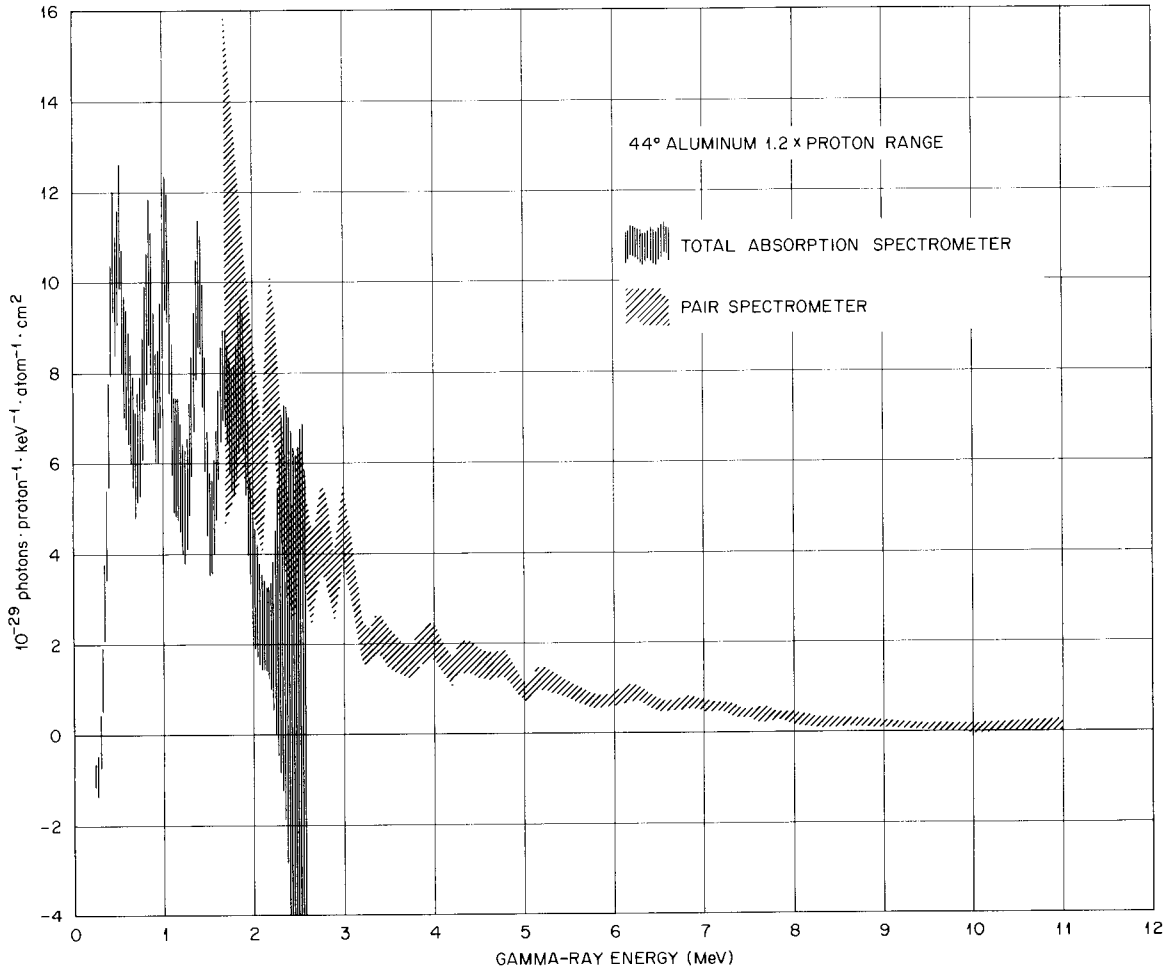


Fig. 32. Absolute Gamma-Ray Yield as a Function of Gamma-Ray Energy Due to the Bombardment by 160-MeV Protons of a 1.2-Proton-Range-Thick Aluminum Target at 44°.

V. Acknowledgments

The authors wish to thank the Office of Naval Research and W. M. Preston of Harvard University for making available the Harvard Synchro-cyclotron for these measurements. A. M. Koehler of Harvard University provided invaluable instruction in the operation of the cyclotron and in the analysis of its output. The mechanical design of the spectrometer was provided by T. F. Sliski and H. J. Stripling. R. T. Santoro carried out the beam monitoring. W. R. Burrus provided extensive assistance in making the first application of his analysis method to "unscrambling" of gamma-ray spectral data. We particularly wish to acknowledge many useful discussions with R. W. Peelle. Finally, we express our appreciation to members of the staff of the Bulk Shielding Facility for their efforts in helping to set up and maintain the equipment required in this experiment.

ORNL-3506
 UC-34 - Physics
 TID-4500 (37th ed.)

INTERNAL DISTRIBUTION

- | | |
|---|----------------------------|
| 1. Biology Library | 209. W. A. Gibson |
| 2-4. Central Research Library | 210. M. L. Halbert |
| 5. Reactor Division Library | 211. F. F. Haywood |
| 6-7. ORNL - Y-12 Technical Library,
Document Reference Section | 212. W. H. Jordan |
| 8-197. Laboratory Records Department | 213. C. E. Larson |
| 198. Laboratory Records, ORNL R.C. | 214. R. S. Livingston |
| 199. G. Dessauer (consultant) | 215. H. H. MacPherson |
| 200. M. L. Goldberger (consultant) | 216-221. F. C. Maienschein |
| 201. R. F. Taschek (consultant) | 222. B. F. Maskewitz |
| 202. R. G. Alsmiller, Jr. | 223. R. Peelle |
| 203. R. Bender | 224. R. T. Santoro |
| 204. E. P. Blizard | 225. M. J. Skinner |
| 205. R. Burrus | 226. J. W. Wachter |
| 206. G. Czjzek | 227. A. M. Weinberg |
| 207. J. K. Dickens | 228. H. A. Wright |
| 208. C. B. Fulmer | 229-278. W. Zobel |

EXTERNAL DISTRIBUTION

279. R. J. Scroggs, Oak Ridge Technical Enterprises Corp., Oak Ridge
280. Marcello Zocchi, Reactor and Radiations Division, National Bureau of Standards, Washington 25, D.C.
281. Edward L. Divita, Radiation Analysis Unit, Martin Nuclear Division, Martin Company, Baltimore 3, Maryland
282. V. B. Bhanot, Physics Department, Panjab University, Chandigarh-3, India
283. Research and Development Division, AEC, ORO
- 284-929. Given distribution as shown in TID-4500 (37th ed.) under Physics category (75 copies - CFSTI)